NONLINEAR MAGNETOELECTRIC EFFECTS IN LAYERED MULTIFERROIC COMPOSITES

Y.K. Fetisov^a and G. Srinivasan^b

^aMIREA – Russian Technological University, Moscow 119454, Russia ^bPhysics Department, Oakland University, Rochester, Michigan 48307, USA

ABSTRACT

Magnetoelectric (ME) effects in a ferromagnetic and piezoelectric composite are changes in the polarization caused by a magnetic field, or changes in the magnetization caused by an electric field. These effects are aided by the mechanical deformation in the ferroic phases caused by the combination of magnetostriction and piezoelectricity. Interest in ME effects is due to a variety of physical phenomena they exhibit, as well as their potential applications in the creation of highly sensitive magnetic field sensors and other electronic devices. Linear ME effects in structures with layers of different ferroic materials have been studied extensively. However, nonlinear ME effects, which are caused by the nonlinearity of the magnetic, dielectric, and acoustic properties of ferromagnets and piezoelectrics, are less well understood. The purpose of this review is to summarize the current state of knowledge on nonlinear ME (NLME) effects in composite heterostructures, and to discuss their potential applications. The review begins by discussing the characteristics of materials that are conductive to the occurrence of NLME effects and ferromagnetic-piezoelectric materials that are most commonly used to study such effects. The review then provides details on theoretical approaches to the description of NLME effects in heterostructures, and experimental methods for studying these effects. Finally, the review presents a chronological overview of the experimentally observed NLME effects in composite structures excited by low-frequency and pulsed magnetic or electric fields. The review concludes with a discussion on the potential applications of NLME effects for highly sensitive magnetic field sensors.

Keywords: magnetoelectric effect, multiferroic heterostructure, ferromagnet, piezoelectric, magnetostriction, piezoelectricity, nonlinear effects, magnetic field sensors.

1. INTRODUCTION

Magnetoelectric (ME) effects in a multiferroic exhibiting both magnetic and ferroelectric orderings manifest as variations in either magnetic and/or electric order parameters. When a magnetic field H is applied to such materials, it polarizes and induces a polarization P (direct ME effect). Similarly, an electric field E applied to the sample results in a variation in the magnetization M (converse ME effect). The existence of ME effects was predicted by Curie in 1894 [1]. The ME effects were first observed in chromium oxide. Astrov reported on the magnetization of a multiferroic under the action of an electric field [2], Rado and Folen observed polarization of a material under a magnetic field [3]. To date, ME effects have been discovered in a number of single-phase multiferroics [4–7]. However, with rare exceptions, the effects in single phase materials are observed either at low temperatures or in high magnetic fields which limits their applications.

A strong, room-temperature ME effect can be realized in a composite comprising a ferromagnetic (FM) and a piezoelectric (PE) phase and is caused by a combination of the magnetostriction and piezoelectric effects in the constituent phases (product property) [8,9]. The direct ME effect under a magnetic field H applied to the composite occurs due to the transfer of magnetostriction induced mechanical deformation to the PE phase and causes the generation of an induced polarization P. In the case of the converse ME effect under E, the deformation of the PE phase due to inverse piezoelectric effect is transferred to the FM phase and the inverse magnetostriction (Villary effect) causes a change in the magnetization M of the sample. ME effects have been studied in detail in a variety of FM-PE composites and under different mechanical connectivity: these include bulk composites [10], layered structures [11,12], thin-film heterostructures [13], and core-shell nanoparticles and fibers [14]. The strength of ME effects, in general, could be measured by applying a low-frequency magnetic h or electric e field in the presence of bias magnetic H or an electric field E and measuring the induced electric or magnetic fields. The field conversion efficiency of the composites increases significantly when the frequency of the excitation field coincides with

the frequency of any acoustic resonance modes of the sample due to a sharp increase in mechanical deformations [15].

Linear ME effects in layered composites with alternating FM and PE phases have been studied in detail. These structures are easy to polarize, and their properties can be controlled by choosing appropriate materials, thicknesses, and geometry of the layers, as well as the orientations of the AC and DC fields [16–18]. The efficiency of the field conversion under the direct ME effect is characterized by the coefficient $\alpha_E = e/h$, where e is the amplitude of the electric field generated in a magnetic field h, and the converse ME effect by the coefficient $\alpha_B = b/e$, where b is the amplitude of the magnetic induction generated by an electric field e. Prototypes of several devices using ME effects have been created. These include highly sensitive sensors of DC and AC magnetic fields [19,20], electronic devices (transformers, inductors, gyrators, antennas) [21-24], devices for information storages [25,26], and energy harvesting [27].

The order parameters of FM and PE materials in the composites are inherently nonlinear. The magnetostriction λ and magnetization M of FM depend nonlinearly on the magnetic field H [28-30] whereas the deformation η and polarization P of PE depend nonlinearly on the electric field E [31, 32]. In addition, the mechanical rigidity and acoustic losses of FM and PE vary nonlinearly when magnetic or electric fields are applied. These nonlinear characteristics lead to a rich variety of nonlinear-ME (NLME) effects in the composites as well.

As is customary in the theory of nonlinear oscillations, nonlinear optics, and nonlinear acoustics, our focus is on the ME effects with characteristics that depend on the amplitude of the excitation magnetic or electric fields [33,34]. In the case of direct-ME effect when the composite is excited with an AC magnetic field, NLME effects arise mainly due to nonlinearities associated with the FM layer. For converse ME effect, however, NLME effects arise due to nonlinearities of both the PE layer and FM layer. The NLME effect, i.e., the generation of fundamental and higher harmonics in the voltage generated when excitated with an AC magnetic field, was first observed

in 2006 [35]. Since then a variety of NLME phenomena have been discovered in composites of various FM and PE materials and theoretical models have been developed for the effects.

In this regard, it is relevant to review the recent advances in the field of NLME effects in layered composites in order to facilitate further investigations into this important phenomenon and open up path ways for device applications based on NLME effects. In this review, we focus only on low-frequency NLME effects under an AC magnetic or electric field. Nonlinear ME effects in the microwave frequencies and magnetization switching or polarization of multiferroic heterostructures with external fields are beyond the scope of this review.

The review is structured as follows: *In section 2*, we discuss the physical mechanism that gives rise to NLME effects. *Section 3* is devoted to theoretical approaches to description of NLME effects in layered composites. *Section 4* of the review describes experimental studies of the effects. *Section 5* of the review provides details on NLME-based highly sensitive sensors for DC and AC magnetic fields. We conclude with directions for further studies of NLME effects in composites and the prospects for their applications in advanced technologies. The review is based on the works of the current authors over the past 20 years as well as other scientific groups involved in research in this area.

2. ME EFFECTS IN LAYERED MULTIFERROIC COMPOSITES

2.1 Linear ME effects

The mechanism of the direct and converse ME effects in composites containing FM and PE layers, as shown in Fig.1, arise as a result of a combination of the magnetostriction of the FM layer and the piezoelectricity of the PE layer and mechanical coupling between them through the interface [8]. The direct ME effect manifests itself as a change in the polarization P of the PE layer under the action of a magnetic field H, and the converse ME effect results in a change in the magnetization M of the FM layer under an electric field E. Although individual FM and PE layers are not magnetoelectric, the interlayer mechanical coupling leads to ME effect.

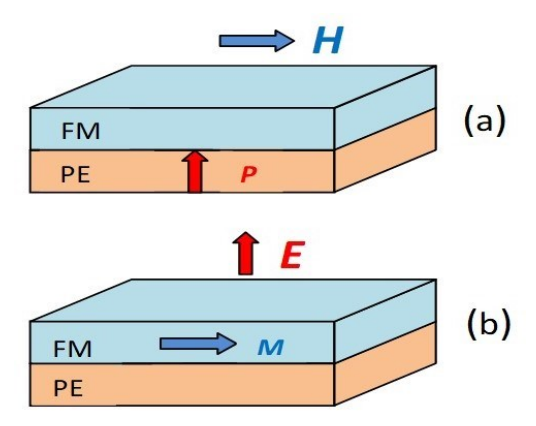


Fig.1 Schematic diagram illustrating direct- and converse magnetoelectric (ME) effects in a bilayer of a ferromagnet (FM) and piezoelectric (PE). (a) Direct ME effect results in an induced ferroelectric polarization due to an applied magnetic field. (b) Converse ME effect leads an induced magnetization in an applied electric field.

Due to finite conductivity of FM and PE layers, ME effects are usually investigated in the dynamic mode when structures are excited by an alternating magnetic or electric field.

In the case of direct ME effect, under the action of alternating magnetic field $h=\delta H\cos(2\pi ft)$ with an amplitude δH and a frequency f, the FM layer of the structure is deformed due to magnetostriction. This deformation when transferred to the PE layer, due to the piezoelectric effect, generates an alternating voltage of the same frequency f and amplitude u. The field conversion efficiency is characterized by the ME coefficient for the direct effect

$$\alpha_E = \left(\frac{\delta E}{\delta H}\right)_{T.H} = \frac{u}{a_m \delta H},\tag{1}$$

where δE is the amplitude of alternating electric field induced by magnetic field δH , u is the amplitude of ME voltage, $a_{\rm P}$ is the thickness of PE layer of the structure. The fields amplitude ratio is taken at a fixed temperature T and bias magnetic field H. The value of the coefficient in the SI system is measured in units of [V/A], and in the CGS system - in units of [V/(cm Oe), while 1 [V/A] ≈ 0.8 [V/(cm·Oe)]. At low amplitudes of the excitation magnetic field h, the amplitude u increases linearly with an increase in δH , which is a criterion for the linearity of the direct ME effect.

In the case of converse ME effect an applied AC electric field $e = \delta E \cos(2\pi ft)$ with amplitude δE and frequency f causes deformation of the PE layer due to inverse piezoelectric effect. This deformation is transferred to the FM layer and, due to inverse magnetostriction (Villari effect), the magnetic induction in the FM layer changes with an amplitude δB and at the same frequency. The efficiency of the field conversion in this case is characterized by the ME coefficient for the converse effect

$$\alpha_B = \left(\frac{\delta B}{\delta E}\right)_{T.E} = \frac{\delta B}{U/a_p},\tag{2}$$

where U is the amplitude of AC voltage applied to the PE layer. The change in the magnetic induction in the FM layer can be measured using a coil wound around the structure. The fields amplitude ratio is taken at a fixed temperature T and bias electric field E. The coefficient α_B is measured in units of [T/(V/cm)] in SI system and in CGS system - in units of [Gs/(V/cm)], while 1 $T/(V/cm) = 10^{-4} Gs/(V/cm)$. For small values of δE , δB increases linearly with increasing δE which is a criterion for the linearity of the converse ME effect.

For the case of small values of δH , δE , and δB , Eq. (1) and (2) can be rewritten as

$$\alpha_E = \left(\frac{\partial E}{\partial H}\right)_{TH} \approx \frac{dE}{dS}\Big|_{TH} \times \frac{dS}{dH}\Big|_{TH} \text{ and } \alpha_B = \left(\frac{\partial B}{\partial E}\right)_{TE} \approx \frac{dB}{dS}\Big|_{TE} \times \frac{dS}{dE}\Big|_{TE}.$$
 (3)

It follows from (3) that for the direct ME effect, α_E is determined by the product of derivatives of the following dependences: E(S) is the dependence of electric field in the PE layer on its deformation and S(H) is the dependence of the FM layer deformation on the magnetic field. For the converse ME effect α_B is determined by the product of derivatives of the dependences: B(S) is the dependence of induction in the FM layer on its deformation and S(E) is the PE layer deformation on the electric field. The derivatives are taken at fixed temperatures and fields. Knowing these characteristics, one can estimate the variations in ME coefficients with H and E fields. To describe nonlinear ME effects, one should consider the nonlinearity of order parameters of FM and PE layers.

2.2 Nonlinearities of order parameters of ferromagnets

The main sources of nonlinearities in ferromagnets are the H-dependence of the magnetostriction $\lambda(H)$, magnetization (or magnetic induction) M(H), and Young's modulus Y(H), and dependence of the magnetization (or magnetic induction) on the strain M(S).

Figure 2a shows typical dependence of $\lambda(H)$ on H for a platelet. As the field H increases from zero, the strain λ increases nonlinearly and reaches the saturation value λ_S as H increases to the saturation field H_S . Moreover, for most ferromagnets in the region of low fields, $H \ll H_S$, magnetostriction depends quadratically on the field $\lambda \sim H^2$ [29]. Upon subsequent decrease in H to zero, λ also drops to zero, and then increases again to saturation when the field direction is reversed. For ferromagnets with hysteresis, the value of the coercive force is H_c . The process is repeated with a cyclic variation of magnetic field. There are ferromagnets with positive magnetostriction $\lambda > 0$, which elongate in the direction of the field, and ferromagnets with negative

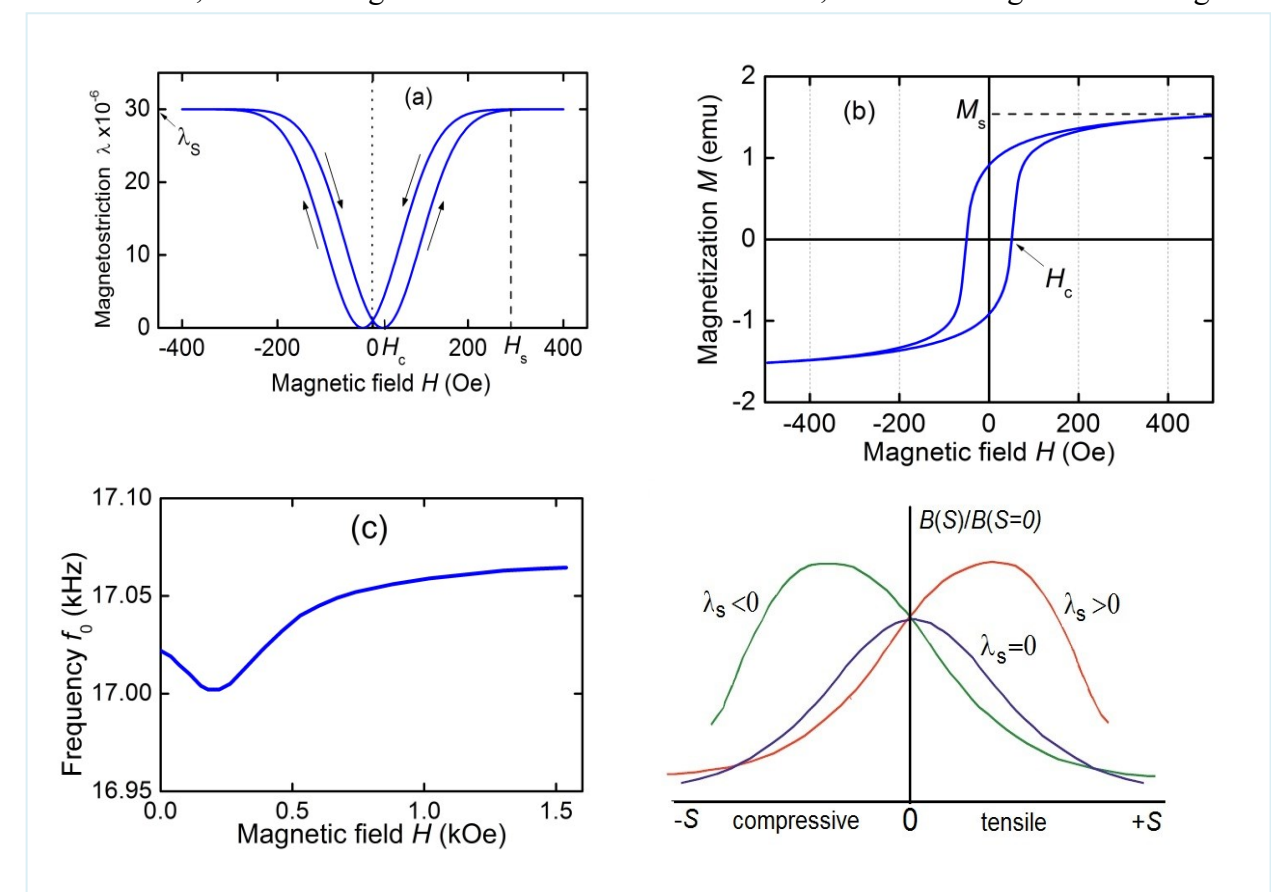


Fig.2 Nonlinear characteristics of ferromagnets: (a) dependence of magnetostriction λ on the magnetic field H, (b) dependence of magnetization M on the field H, (c) dependence of resonant frequency f_0 on the field H, (d) dependence of magnetic induction B on the strain S,

magnetostriction, λ <0, which shrink in the direction of the field. In single-crystal ferromagnets, the magnetostriction is anisotropic and depends on the direction of the field H with respect to the crystallographic axes of the crystal. The shape of the magnetostriction curve and values of the characteristic parameters of the curve depend on the dimensions of the sample, temperature, and pretreatment of the material.

Figure 2b shows a typical nonlinear dependence of the magnetization M on the field H [36]. The slope of M vs H in low fields determines value of the relative permeability μ of the ferromagnet. Obviously, nonlinear dependence of B on H leads to a nonlinear dependence of the differential magnetic permeability of ferromagnet on the field.

Let us add that in the region of low fields $H \ll H_S$, the quadratic dependence of magnetostriction λ on field H (Fig. 2a) and the linear dependence of magnetization M on field H (Fig. 2b) lead to a quadratic dependence of magnetostriction on magnetization $\lambda \sim M^2$ [30].

The application of magnetic field H to the ferromagnetic sample causes a rearrangement of its domain structure, leading to a change in its mechanical rigidity (Young's modulus Y). This manifests as dependence of acoustic resonance frequency on H since $f_0(H) \sim \sqrt{Y(H)}$. Figure 2c shows typical dependence of the planar resonance frequency $f_0(H)$ on H for a sample in the form of a plate [37]. For most ferromagnets, the change in f_0 does not exceed fraction of a percent. However, for weak antiferromagnets with an easy-plane anisotropy (for example, hematite α -Fe₂O₃ and iron borate FeBO₃), the change in frequency under the action of magnetic field can reach tens of percent [38].

Finally, the magnetic induction B in a ferromagnet depends nonlinearly on the deformation S (inverse magnetostriction or the Villari effect). Figure 2d shows typical dependence of the normalized induction B(S)/B(S=0) for ferromagnets with either positive or negative magnetostriction. For $\lambda > 0$, the induction B increases with stretching (S > 0), reaches a maximum, and then drops. For ferromagnets with $\lambda < 0$, the induction reaches its maximum when the sample is compressed.

In this case, the change δB under the action of deformation is, as a rule, small and depends on the initial state of the sample [39].

Table 1 lists typical parameter values for magnetostrictive materials, with the Curie temperature T_c above room temperature, that are most often used in ME composites.

TABLE 1. Characteristics of some magnetostrictive materials

Material	$\lambda_{\rm S} \times 10^6$	Hs, Oe	H _c , Oe	Bs, T	$\mu_{ ext{max}}$	Y, GPa	Ref.
Ni	-35	~500	~20	-	~100	215	[36]
FeCoV	80	~2000	~40	~0.9	~12	210	[36]
Metglas	27	~100	<0.5	1.56	$\sim 10^4 - 10^5$	~100	[41]
Galfenol	~300	~200	~20	~1.6	~100	~70	[42]
Terfenol-D	1200	~2000	~100	~1	~10	~80	[43]
NZFO ferrite	-24	~1000	~100	~0.2	~500	140	[44]
CZFO ferrite	-60	~2000	~1000	-	160	280	[44]

Ni and Co and alloys based on them (FeCoV- permendur for example) have a large λ and are saturated in relatively low magnetic fields [36]. For Ni λ is negative whereas it is positive for FeCoV. Metglas, an amorphous alloy of the composition FeBSiC, in the form of 20–30 μ m thick ribbons [40] and thin films [41] also have a large magnetostriction, but they are saturated in very low fields and have a low H_c value. Alloys of the composition Fe_{1-x}Ga_x (galfenol) also have a very large λ and a small saturation field [42]. Rare-earth alloys of the composition Tb_xDy_{1-x}Fe₂, (Terfenol-D) have the highest λ , but the saturation occurs at very high magnetic fields, have a rather large hysteresis, and are difficult to process [43]. Ferrimagnetic oxides, for example, Ni-Zn-ferrites (Ni_{1-x}Zn_xFe₂O₄) and Co-Zn-ferrites (Co_{1-x}Zn_xFe₂O₄) are dielectrics and also have large λ values [44]. Magnetic fiber composites (MFC) containing a magnetostrictive material in a polymer matrix are also of interest for use in ME composites [45].

2.3 Nonlinearities of order parameters of piezoelectrics

The main sources of nonlinearities in piezoelectrics are the nonlinear E-dependence of deformation $\eta(E)$, polarization P(E) (or electric induction D(E)), and the mechanical rigidity (Young's modulus Y(E)). In addition, dependence of P on strain S is also nonlinear.

Figure 3a shows typical dependence of η on E for a ferroelectric platelet polarized perpendicular to the plane [46]. As E increases from zero, η increases approximately linearly and tends to saturation at saturation field E_S . Then, as E decreases the deformation η drops to zero, changes sign when E is reversed, then abruptly switches sign at E_S and increases again as E increases.

Hysteresis in piezoelectrics arises due to the rearrangement of the domain structure. There are piezoelectrics show either elongation or contraction when an electric field is applied. In single crystals, the piezoelectric effect has a strong anisotropy. The shape of the deformation η vs E and values of the characteristic parameters depend on the temperature and pretreatment of the material as well as on the rate of electric field tuning, since the process of repolarization usually is rather

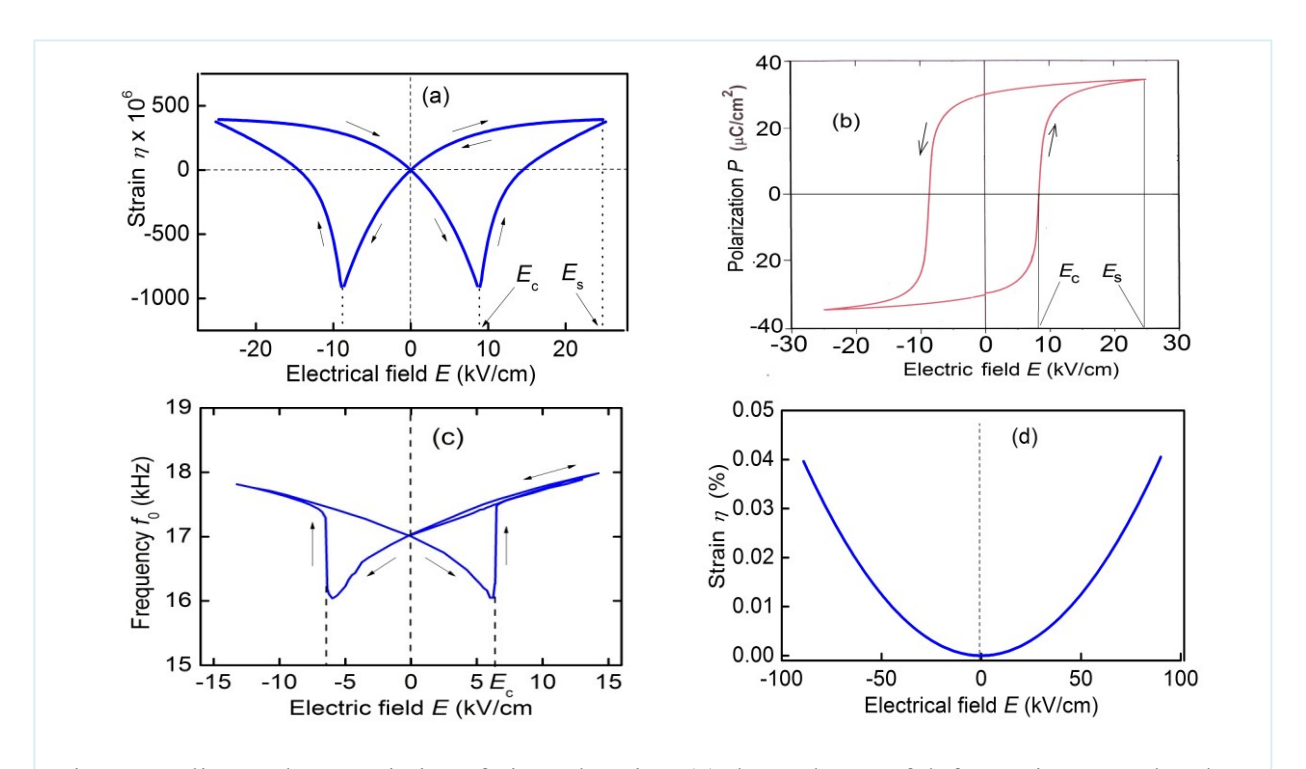


Fig. 3 Nonlinear characteristics of piezoelectrics: (a) dependence of deformation η on the electric field E, (b) dependence of polarization P on the field E, (c) dependence of resonant frequency f_0 on the field E, (d) deformation η vs. electric field E for electrostrictors.

slow. The magnitude of the piezoelectric deformation is characterized by the piezoelectric modulus which is equal to the slope $d \approx \partial \eta / \partial E$ in the low field region of η vs E. Parameters of piezomaterials vary depending on the composition, but the table shows typical values.

Figure 3b shows typical dependence of P on E [46]. The saturation field E_S and the repolarization field E_C of the piezoelectric are the same as for the η vs E dependence. The slope of the variation in the low field region determines value of the initial relative permittivity $\varepsilon \approx D/E$. Obviously, the nonlinear dependence of electric induction on the field leads to a nonlinear dependence of the differential permittivity of the dielectric on the field $\varepsilon(E) = \partial D/\partial E$.

The mechanical stiffness (Young's modulus Y) of piezoelectrics also depends on E. Figure 3c shows typical acoustic resonance frequency f_0 vs E dependence that varies as $f_0(E) \sim \sqrt{Y(E)}$ for a piezoelectric plate. The change in f_0 is due to a change in Y, it reaches ~20% and it tracks the butterfly curve-like dependence of the deformation on the field $\eta(E)$ [47].

Table 2 lists typical parameter values for piezoelectric materials, that are most often used in ME composites.

TABLE 2. Characteristics of some piezoelectric materials

Material	<i>d</i> ₃₃ , pC/N	E _S , kV/cm	E _c , kV/cm	ε	Q	Y, GPa	Ref.
PMN-PT ceramic or crystal	600- 20000	~10	~5	4000	$\sim 10^2 - 10^4$	56	[48]
Piezoceramics PZT	400	~25	~10	1800	~10 ²	70	[49]
Piezopolymer PVDF-Fr film	18	~2000	~400	10	~10-10 ²	~1	[50]
Langatate crystal	5.2	-	-	23	~104	~110	[51]
Quartz crystal	2.4	-	-	6.8	~106	~80	[52]
Aluminium nitride films	~6	-	-	10	~104	140	[53,54]
Piezo-fiber composites (PFC)	400	-	-	~160	~10-10 ²	~300	[55]

The first three materials, lead magnesium titanate – lead titanate ceramics or crystals Pb(Mg_{1/3}Nb_{2/3})O₃–PbTiO₃ (PMN-PT) [48], lead zirconate titanate ceramics Pb_{0.48}Zr_{0.52}TiO₃ (PZT) [49], and piezopolymer films PVDF-Fr [50] belong to ferroelectrics with Curie temperature above room temperature. PMN-PT has the highest piezoelectric modulus d_{33} among all materials, a high dielectric permittivity ε , and a relatively narrow repolarization loop P(E). Piezopolymer films PVDF-Fr have a small d_{33} , a wide repolarization loop and the lowest Young's modulus [49]. Single crystals of languate La₃Ga_{5.5}Ta_{0.5}O₁₄ (LGT) [51], quartz (SiO₂) [52], and aluminum nitride (AlN) [53,54] are piezoelectrics, they possess a linear dependence of deformation vs. electric field $\eta \sim d$ x E, small piezoelectric modulus and dielectric permittivity, and have no hysteresis. Flexible piezo-fiber composites (PFCs) comprising PZT or PMN-PT fibers in a polymer matrix have a high piezoelectric modulus and widely used in ME heterostructures [55]. Among the listed materials, the single crystals have the highest acoustic quality factor Q, which increases the ME effect at acoustic resonance frequencies.

We should add that in composite heterostructures, instead of a piezoelectric, one can use electrostrictive materials [56]. Figure 3d shows typical dependence of electrostrictor's deformation vs. applied electric field. The deformation usually increases quadratically with increasing field $\eta \sim E^2$. Deformation of an electrostrictive material leads to a change in its permittivity, but does not cause the generation of electrical charges [57].

3. THEORY OF NONLINEAR ME EFFECTS

3.1 Nonlinear direct ME effects

In the case of direct ME effect, when the composite is excited by an alternating magnetic field, the main reason for the appearance of nonlinear ME effects is the nonlinear dependence of the FM layer magnetostriction on the field $\lambda(H)$ (see Fig. 1a). To describe the nonlinear direct ME effect we use an approach developed in Refs. [58,59]. We consider a planar symmetric as well as an asymmetric FM-PE heterostructures. The symmetrical trilayer contains a PE layer of a thickness

of a_p , located between two FM layers of a thickness $a_m/2$ each. The asymmetric structure contains a PE layer of a thickness a_p and an FM layer of a thickness a_m . Thin electrodes are assumed on the surfaces of the PE layer, across which the generated ME voltage u is measured. The layer length is L and the width is b. The layer thickness is assumed to be much smaller than L and b. The composite is in (1,2) plane, axis a is directed perpendicular to the plane. The polarization in the PE layer is directed along axis a and an external DC magnetizing field a is directed parallel to the plane along axis a.

Deformation S, mechanical stress T, magnetic field H inside the FM layers, electric field E and electric induction D in the PE layer are related to each other by the following relations (in CGS)

$$S_1^P = S_{11}^p T_1^p + d_{31} E_3 (4a)$$

$$S_1^m = s_{11}^m T_1^m + \lambda_{11}(H) \tag{4b}$$

$$D_3 = d_{31}T_1^p + \varepsilon E_3 \tag{4c}$$

Indices p and m in Eq. (4) represent the PE and FM layers, respectively. $\lambda_{11}(H)$ is the longitudinal magnetostriction of the FM layer, d_{31} is the piezoelectric coefficient of the PE layer, s_{11}^p and s_{11}^m are the compliances of the materials, and ε is the relative permittivity of the PE layer.

Consider first the symmetric trilayer composite. Under the field H, it is deformed only in the (1,2) plane. In this case, the deformations S_1^p and S_1^m are homogeneous over the thickness. Using Eq. (4), the condition of continuity of deformation at the interface between the layers $S_1^p = S_1^m$ and the condition of the structure equilibrium along axis I: $a_p T_1^p + a_m T_1^m = 0$ we obtain an expression for the mechanical stress T_1^p in the PE layer. By virtue of our assumptions, the electric field in the PE layer is directed along axis 3 and is uniform. Then an additional condition $D_3^p = 0$ follows from Maxwell's equation divD = 0. Finally, the voltage u generated between electrodes of the PE layer is given by:

$$u = E_3 a_p = -\frac{d_{31} \lambda_{11}(H) a_p}{\varepsilon [s_{11}^p + (a_p / a_m) s_{11}^m] - d_{31}^2} \approx A d_{31} \lambda_{11}(H).$$
 (5)

The term d_{31}^2 in Eq.(5) is small and can be neglected.

The asymmetric FM-PE structure, in additional to longitudinal deformation, will also undergo a bending under the action of a magnetic field leading to the terms $S_1^p(z)$ and $S_1^m(z)$ that vary linearly with thickness. A neutral plane with S=0 must be present inside the structure at some distance from the interface. Using Eq.(4), and the condition of equilibrium along axis I, and the condition of equilibrium with respect to rotation around axis 2 through the neutral plane, we obtain an expression for the distribution of mechanical stresses in the PE layer $T_1^p(z)$. Then, using the open loop condition $D_3^p=0$, we find the field distribution $E_3(z)$ in the PE layer. Finally, integrating $E_3(z)$ over the layer thickness a_p , we obtain an expression for the voltage u generated

$$u = Gd_{31}\lambda_{11}(H). \tag{6}$$

An explicit expression for the coefficient G is given, for example, in Ref. [58]. The coefficients A and G in Eqs. (5) and (6) depend only on composite dimensions and mechanical and electrical properties of the layers. For more complex structures containing several FM and PE layers, the expressions for u will have the same form as Eqs.(5) and (6), but with different coefficients. We emphasize that for all ME structures the voltage is a linear function of magnetostriction $u \sim \lambda_{11}(H)$.

Next, we consider the response of the composite to an applied magnetic field $H(t) = H_0 + h \cdot \cos(2\pi f t)$, where H_0 is the DC bias field and $h(t) = h \cos(2\pi f t)$ is the AC field. One may then expand $\lambda(H)$ as a Taylor series up to the fourth order near the field H_0 under the condition $h \ll H_0$:

$$\lambda(H) = \lambda(H_0) + \sum_{n=1}^{4} \frac{1}{n!} \lambda^{(n)} [h \cos(2\pi n f t)]^n , \qquad (7)$$

where $\lambda^{(n)} = \partial^n \lambda / \partial H^n \Big|_{H_0}$ is the n-th order derivative of λ with respect to $H=H_0$ and n=1,2,3... Terms $\lambda^{(1)}$ is the piezomagnetic modulus and $\lambda^{(2)}$ is the nonlinear piezomagnetic modulus. Substituting Eq. (4) in Eq. (2), we obtain:

$$u = u_0 + u_1 \cos(2\pi f t) + u_2 \cos(4\pi f t) + u_3 \cos(6\pi f t) + u_4 \cos(8\pi f t) + \dots$$
 (8)

In Eq. (8), the magnitude of the DC voltage is given by

$$u_0 = Ad_{31}[\lambda(H_0) + (1/4)\lambda^{(2)}h^2 + (1/64)\lambda^{(4)}h^4], \tag{9a}$$

and the amplitudes of harmonics with frequencies nf are given by the following expressions:

$$u_1 = Ad_{31}[\lambda^{(1)}h + (1/8)\lambda^{(3)}h^3], \tag{9b}$$

$$u_2 = Ad_{31}[(1/4)\lambda^{(2)}h^2 + (1/48)\lambda^{(4)}h^4], \tag{9c}$$

$$u_3 = Ad_{31}(1/24)\lambda^{(3)}h^3, \tag{9d}$$

$$u_4 = Ad_{31}(1/192)\lambda^{(4)}h^4. (9f)$$

The DC voltage u_0 (Eq. 6a) is expected to decrease rapidly to zero due to the finite conductivity of the PE layer, so we will not consider it further. It follows from Eq. (9b)-(9f) that $u_n \sim \lambda^{(n)}$, and the higher order derivatives make a small additional contribution to the u_n . The H-dependence of $u_n(H)$ is determined by the field dependence of corresponding derivative $\lambda^{(n)}(H)$ and the dependence of u_n on h is given by $u_n \sim h^n$.

A special case of interest when the composite is simultaneously excited by two AC magnetic fields with amplitudes h_1 and h_2 and frequencies f_1 and f_2 :

$$h(t) = h_1 \cos(2\pi f_1 t) + h_2 \cos(2\pi f_2 t). \tag{10}$$

Using Eqs.(5) and (7) and restricting ourselves to terms of the second order, we obtain an expression for the generated ME voltage:

$$u = u_0 + u_1^{(1)} \cos(2\pi f_1 t) + u_2^{(1)} \cos(2\pi f_2 t) + u_1^{(2)} \cos(4\pi f_1 t) + u_2^{(2)} \cos(4\pi f_2 t) + u_{mix} \cos[2\pi (f_1 + f_2)t] + u_{mix} \cos[2\pi (f_1 - f_2)t].$$

$$(11)$$

In Eq.(11) the lower index corresponds to the frequency (f_1 or f_2), and the upper index corresponds to the order of the harmonic (order of the derivative n).

The DC voltage amplitude in Eq.(11) is given by:

$$u_0 = Ad_{31}[\lambda(H_0) + (1/4)(h_1^2 + h_2^2)]$$
(12a)

The amplitudes of the first and second harmonics are given by:

$$u_1^{(1)} = Ad_{31}\lambda^{(1)}(H_0)h_1$$
 and $u_2^{(1)} = Ad_{31}\lambda^{(1)}(H_0)h_2$ (12b)

$$u_1^{(2)} = (1/4)Ad_{31}\lambda^{(2)}(H_0)h_1^2$$
 and $u_2^{(2)} = (1/4)Ad_{31}\lambda^{(2)}(H_0)h_2^2$ (12c)

Amplitude of the voltage with frequencies $f_1 \pm f_2$:

$$u_{mir} = (1/4)Ad_{31}\lambda^{(2)}(H_0)h_1h_2. \tag{12d}$$

Thus, from equations Eqs. (8)-(11) it follows that the nonlinear dependence of the FM layer magnetostriction on the field $\lambda(H)$ should lead to the following nonlinear ME effects:

- generation of a DC voltage u_0 under the action of an AC magnetic field (useful for realizing a sensor of AC magnetic field);
- generation of voltages u_n with frequencies $f_n=nf$, harmonics of the excitation magnetic field f (harmonic generation);
- generation of voltages u_{mix} with combination frequencies when the structure is excited by two magnetic fields with different frequencies (magnetic sensors).

To characterize the efficiency of field conversion by direct NLME effect, the following coefficients are introduced: linear ME modulus $\alpha_E^{(1)} = u_1/(a_p h)$, nonlinear ME moduli $\alpha_E^{(2)} = u_2/(a_p h^2)$ and $\alpha_E^{mix} = u_{mix}/(a_p h_1 h_2)$.

It follows from Eqs.(9b) and (9c) that the dependence of the linear ME coefficient on the field H is determined mainly by the field dependence of the piezomagnetic modulus $\alpha_E^{(1)}(H) \sim \lambda^{(1)}(H)$, and the dependence of the NLME coefficient on H is mainly determined by the field dependence of the nonlinear piezomagnetic modulus $\alpha_E^{(2)}(H) \sim \lambda^{(2)}(H)$. In the calculations of the amplitudes of harmonics, it is best to use the derivatives $\lambda^{(2)}(H)$, found by numerical differentiation of the dependence $\lambda(H)$ measured for a specific structure. It is also possible to estimate the dependence by an analytical function of the form $\lambda(H) = \lambda_S [1 - \exp(-\beta H^2)]$, (where β is an adjustable coefficient) which assumes a quadratic dependence of the magnetostriction on H, $\lambda \approx \beta \cdot H^2$ in low fields, and describes saturation of the magnetostriction at the level λ_S in high fields [59]. In a limited range of fields, the dependence $\lambda(H)$ can be approximated using a polynomial [60]. We also note the work in Ref.[61], where the method of expanding $\lambda(H)$ in a Taylor series was used to describe direct NLME effect.

3.2 Nonlinear converse ME effect

In the case of converse ME effect, when the composite is excited by an AC electric field, the NLME effects are caused, first of all, by nonlinear dependence of the piezoelectric strain in the PE layer on E (Fig. 3a). To describe the converse NLME effects, we use an approach similar to the direct NLME effect. For a symmetric composite, strain S, mechanical stress T, magnetic induction B_1 and magnetic field H_1 inside the FM layers and electric field E_3 in the PE layer are given by:

$$S_1^P = S_{11}^p T_1^p + \eta_{31}(E_3) \tag{13a}$$

$$S_1^m = s_{11}^m T_1^m + \lambda_{11}^{(1)} H_1 \tag{13b}$$

$$B_1 = \lambda_{11}^{(1)} T_1^m + \mu \cdot H_1 \tag{13c}$$

The indices p and m in Eq.(13) represent, as before, to PE and FM layers, $\eta_{31}(E_3)$ is the deformation of the PE layer along direction I under the action of field E_3 , $\lambda_{11}^{(1)}$ is the piezomagnetic modulus of

the FM layer, S_{11}^p and S_{11}^m are the compliance of materials, μ is the relative magnetic permeability of the FM layer.

Using Eq.(13), the condition of continuity of deformation at the interfaces and condition of equilibrium of the composite along axis I: $a_p T_1^p + a_m T_1^m = 0$, we obtain an expression for T_1^m in the FM layer. In addition, it follows from the Maxwell equation Div(B) = 0 that in the FM layer $B_1 = 0$. Finally, we obtain the following expression for H_1 in the FM layer:

$$H_{1} = -\frac{\lambda_{11}^{(1)} \eta_{31}(E)}{\mu \left[s_{11}^{m} + (a_{m}/a_{p})s_{11}^{p}\right] - (\lambda_{11}^{(1)})^{2}} = C\lambda_{11}^{(1)} \eta_{31}(E).$$
(14)

Equation (14) has the same form as Eq.(5) for the direct ME effect, but with a different coefficient C. Magnitude of the field generated depends linearly on the piezo deformation $H_1 \sim \eta(E)$.

Next, we choose an electric field of the form $E(t) = E_0 + e \cos(2\pi f t)$ and expand the deformation in a Taylor series in terms of the amplitude of the excitation field e near E_0 under the condition $e << E_0$,

$$\eta(E) = \eta(E_0) + \sum_{n=1}^{4} \frac{1}{n!} \eta^{(n)} [e \cos(2\pi n f t)]^n , \qquad (15)$$

Substituting Eq.(15) into (14) and restricting ourselves to terms up to the second order, we obtain an expression for the magnetic field in the FM layer:

$$h = h_0 + h_1 \cos(2\pi f t) + h_2 \cos(4\pi f t)... \tag{16}$$

In Eq. (16), value of DC magnetic field is given by:

$$h_0 = C\lambda_{11}^{(1)} [\eta(E_0) + (1/4)\eta^{(2)}h^2], \tag{17a},$$

and amplitudes of the first and second harmonics of the field are given by

$$h_1 = C\lambda_{11}^{(1)}\eta^{(1)}e,$$
 (17b),

$$h_2 = C\lambda_{11}^{(1)}(1/4)\eta^{(2)}e^2$$
. (17c),

In Eq.(17) $\eta^{(1)} = \partial \eta / \partial E \big|_{E_0} = d_{31}$ is the linear piezoelectric modulus, $\eta^{(2)} = \partial^2 \eta / \partial E^2 \big|_{E_0}$ is the nonlinear piezoelectric modulus.

If the composite is excited by two electric fields with frequencies f_1 and f_2

$$e(t) = e_1 \cos(2\pi f_1 t) + e_2 \cos(2\pi f_2 t), \tag{18}$$

then magnetic fields with sum and difference frequencies are generated in the FM layer

$$h(t) = h_{mix} \cos[2\pi (f_1 + f_2)] + h_{mix} \cos[2\pi (f_1 - f_2)]$$
(19)

with an amplitude of $h_{mix} = (1/4)C\lambda_{11}^{(1)}\eta^{(2)}e^2$.

Thus, in the case of converse ME effect, the nonlinear dependence of the piezoelectric strain on the electric field $\eta(E)$ should lead to the following nonlinear ME effects: generation of a DC magnetic field h_0 , generation of magnetic field h_2 with a doubled frequency, and generation of magnetic fields h_{mix} with combination frequencies. To characterize the efficiency of the field conversion in the case of converse NLME effect, one can introduce the coefficients: linear ME coefficient $\alpha_B^{(1)} = \mu h_1/e$, nonlinear ME coefficients $\alpha_B^{(2)} = \mu h_2/e^2$ and $\alpha_B^{\text{mix}} = \mu h_{\text{mix}}/(e_1 e_2)$. It follows from Eq. (17b) and (17c) that the dependence of the linear ME coefficient on E is determined by piezoelectric modulus $\alpha_B^{(1)}(E) \sim \eta^{(1)}(E)$ and dependence of the nonlinear ME coefficients on E is determined by nonlinear piezoelectric moduli $\alpha_B^{(2)}(E)$, $\alpha_B^{\text{mix}}(E) \sim \eta^{(2)}(E)$. In addition, both the coefficients depend on the magnetic field E due to the field dependence of the piezomagnetic modulus $R_{11}^{(1)}(H)$.

3.3 Features of nonlinear ME effects

It is clear from the discussion so far that the strength of the direct NLME effect is determined mainly by the value of $\lambda^{(2)}(H)$ and that the strength of the converse NLME effect is determined by

the value of $\eta^{(2)}(E)$. By differentiating λ vs H as in Fig. 2a and η vs E as in Fig. 3a, one can find the field dependences of the magnitude of NLME effects. As an example, Fig. 4 shows typical dependences of λ (measured with a strain gage) and its derivatives $\lambda^{(1)}$ and $\lambda^{(2)}$ on H for an in-plane magnetized ferromagnetic Metglas platelet.

For the FM layer, the first derivative $\lambda^{(1)}$ determines the H dependence of the linear direct ME effect, $\alpha_E^{(1)}(H) \sim \lambda^{(1)}(H)$. In the absence of hysteresis, $\lambda^{(1)}$ is zero at H=0, reaches a maximum at a characteristic field H_m , and then tends to zero when the ferromagnet is saturated. The second derivative $\lambda^{(2)}$ determines the H dependence of the direct NLME effect $\alpha_E^{(2)}(H) \sim \lambda^{(2)}(H)$. The second derivative, on the contrary, is maximum in the absence of a bias field, vanishes at the same field H_m , passes through the second maximum with an increase in H, and only then tends to zero.

Figure 5 shows typical dependences of the piezoelectric strain η measured by an optical method when E was scanned at 1 Hz and its derivatives $\eta^{(1)}$ and $\eta^{(2)}$ on E for a transversely poled PZT platelet. For the PE layer, $\eta^{(1)}$ determines E dependence of the magnitude of the converse linear ME effect $\alpha_B^{(1)}(E) \sim \eta^{(1)}(E)$. It can be seen that $\eta^{(1)}$ is small for fields from zero to the polarization reversal field E_c , then it sharply increases near E_c and falls again with increasing field. The second derivative $\eta^{(2)}$ determines the magnitude of the NLME effect $\alpha_B^{(2)}(E) \sim \eta^{(2)}(E)$. It is small over the entire range of E and increases only near the polarization reversal field E_c .

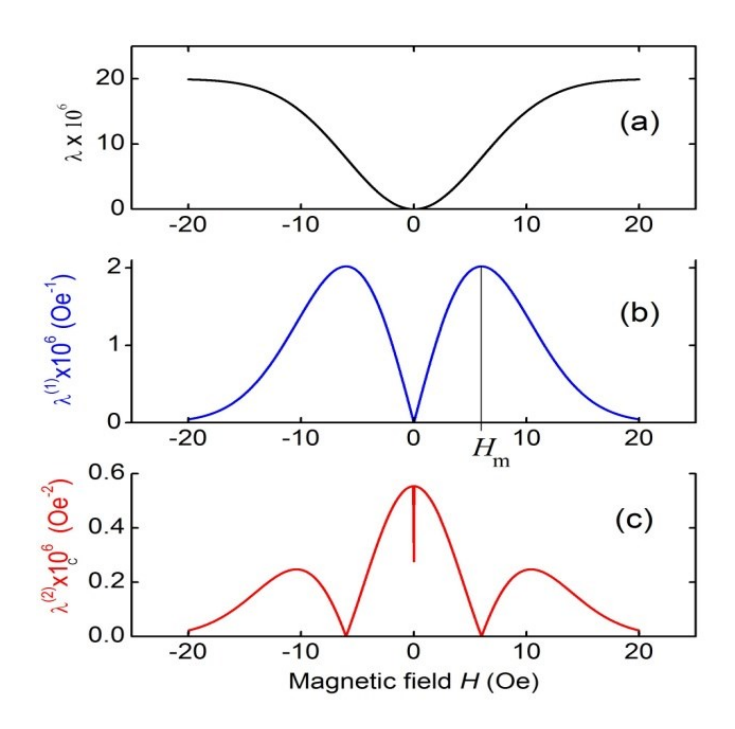


Fig. 4 Dependences of (a) the magnetostriction λ , (b) its first derivative $\lambda^{(1)}$ and (c) its second derivative $\lambda^{(2)}$ on the magnetic field H for an in-plane magnetized Metglas layer.

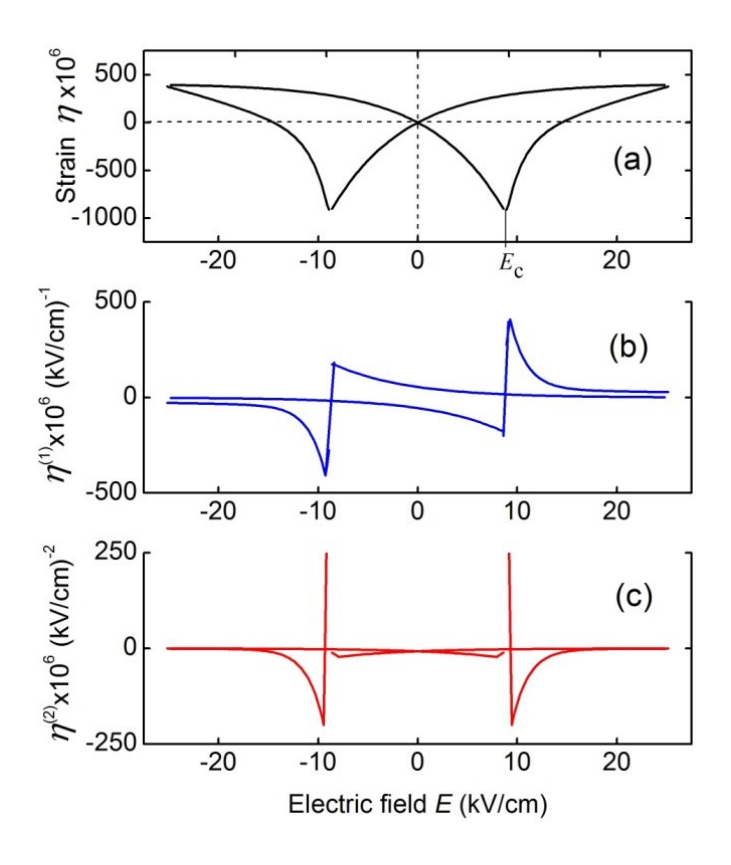


Fig.5. Dependences of (a) the piezoelectric strain η , (b) its first derivative $\eta^{(1)}$ and (c) its second derivative $\eta^{(2)}$ on the electric field E for a transversely poled PZT platelet.

Comparison of the variations in $\lambda^{(2)}$ and $\eta^{(2)}$ with H and E, respectively, allows us to make the following conclusions concerning NLME effects in FM-PE composites:

- Direct NLME effects in composite FM-FE heterostructures could be observed either in the absence or in a weak DC bias magnetic field;
- Converse NLME effects in composite heterostructures with FE layers are weak in the absence or in a weak DC *E*-field and can generally be observed only for fields $E\approx E_c$;
- Converse NLME effect can also arise in composite FM-FE heterostructures due to nonlinearity of FM layer at large amplitudes of AC *e*-field and AC *h*-field.
- In composite heterostructures with electrostrictive layers, the direct NLME effect should be absent, because deformation of the electrostrictor does not lead to generation of electrical voltage. Magnitude of the converse NLME effect should not depend on the DC *E*-field, but will change with a change in the DC *H*-field.

For both direct and converse NLME effects, the strengths of the ME response increases by a factor of acoustic quality factor of $Q \sim 10^2$ -10³ when the frequency of the excitation field or frequency of the ME voltage coincides with the acoustic resonance frequencies. The resonance frequencies depend on the composite geometry/dimensions, thicknesses, and mechanical parameters of the layers [62]. For example, for a rectangular sample of length L and thickness a, the frequencies of longitudinal f_1 and bending f_2 vibration modes are given by:

$$f_1 \approx \frac{1}{2L} \sqrt{\frac{Y_{ef}}{\rho_{ef}}}$$
 and $f_2 \approx \frac{k^2}{2\pi} \frac{a}{2L^2} \sqrt{\frac{Y_{ef}}{\rho_{ef}}}$. (20)

Here, the effective values of Young's modulus and density should be used:

$$Y_{ef} = \sum_{i} Y_{i} a_{i} / \sum_{i} a_{i}$$
 и $\rho_{ef} = \sum_{i} \rho_{i} a_{i} / \sum_{i} a_{i}$, $a = \sum_{i} a_{i}$, where Y_{i} and ρ_{i} are the Young's moduli and layer densities, respectively, a_{i} is the thickness of the i -th layer, k is the coefficient for a given vibration mode. When estimating the characteristics of NLME effects, it is necessary to take into account demagnetization that will lead to a decrease in both DC and AC magnetic fields,

$$H \approx H_{ex} - N \cdot M \approx \frac{H_{ex}}{1 + (\mu - 1)N},\tag{21}$$

where H_{ex} is the applied DC field, N is the demagnetizing factor, M is the magnetization of the sample, and μ is the initial magnetic permeability of the material [63,64]. The discussion so far is applicable to assumed orientations of P, E, e, H, and H. For other orientations the coefficients in Eqs. (5) and (14) will have to be estimated [65,66]. Also for large amplitudes of the excitation fields, $h\sim H$ or $e\sim E$, expanding the strain in a Taylor series is not valid.

4. EXPERIMENTAL INVESTIGATION OF NONLINEAR ME EFFECTS

4.1 Methods for investigating nonlinear effects

A block-diagram of typical setup for studying NLME effects is shown in Fig. 6 [67]. For direct ME effect, the sample is subjected to both a DC and AC magnetic fields. The AC voltage generated across PE layer is fed to an oscilloscope and a spectrum analyzer to record its amplitude and frequency spectrum. For converse ME effect, the same setup can be used, but an AC voltage is applied across the electrodes of the PE layer to establish an electric field and the voltage generated in the pickup coil is fed to the oscilloscope and spectrum analyzer.

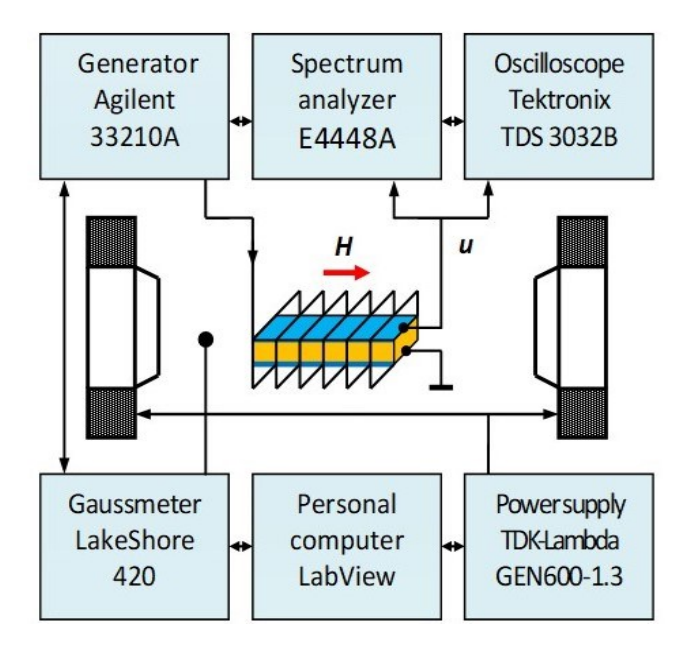


Fig.6. Block-diagram of the setup for studying nonlinear ME effects in heterostructures.

In experiments, the NLME effects can manifest in several ways. To illustrate, we give examples for the direct NLME effect in Figure 7:

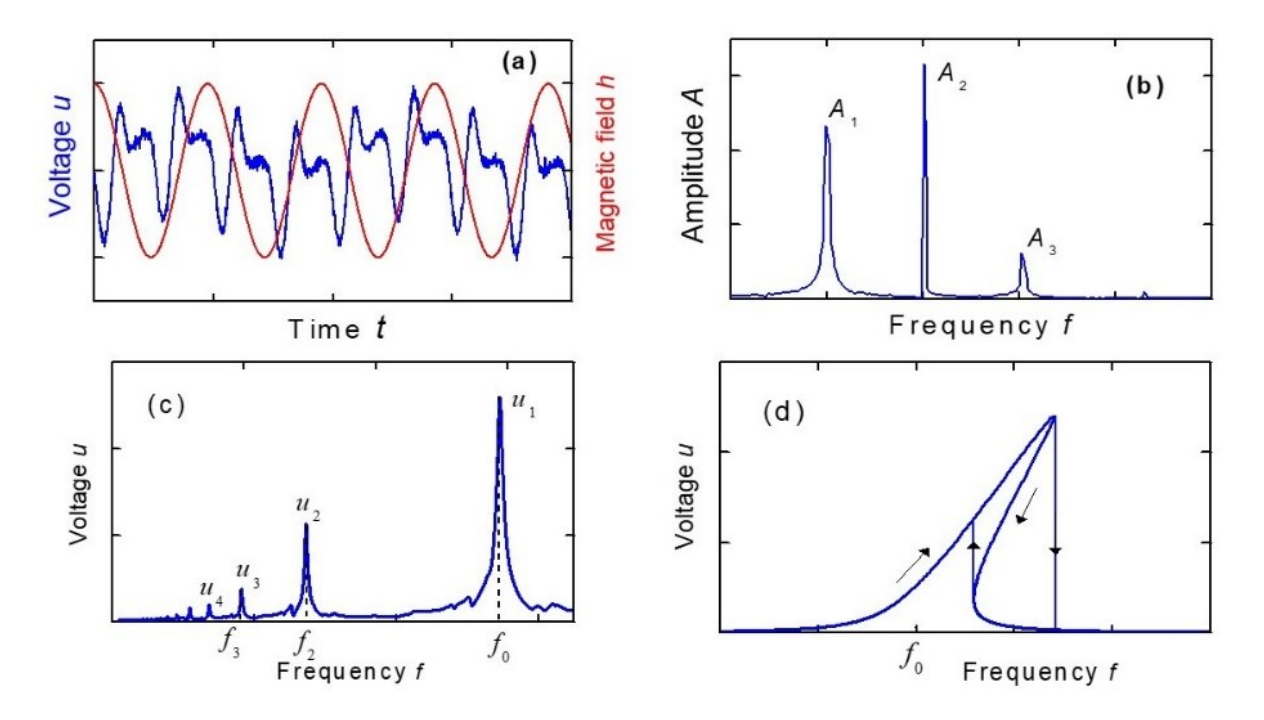


Fig. 7 Manifestations of nonlinearity of the direct ME effect in composite heterostructures with an increase in the amplitude of the excitation magnetic field h: (a) distortion of the generated voltage waveform, (b) enrichment of the frequency spectrum of the generated voltage, (c) change in the shape of the amplitude-frequency response, (d) distortion of the shape of the resonance curve and appearance of hysteresis. Here f is the frequency of the applied h field.

- a) With an increase in the amplitude of h at f_0 the shape of the generated ME voltage u(t) is distorted as in Figure 7a due to the excitation of harmonics.
- b) The distortion of u(t) is accompanied by higher harmonics at $f_n = nf_0$ (where n=2,3,4...) as shown in Fig.7b. One may also observe subharmonics with frequencies $f_n = f_0/n$ (where n=2,3,4...). When subjected to two or more AC fields one may observe ME voltages at combination frequencies or a continuous noise spectrum.
- c) As h increases, the shape of the amplitude-frequency response due to NLME may change. Figure 7c shows the dependence of u on f measured by a broadband diode during frequency scanning. At small h, the frequency response exhibited a single peak u_1 at f_1 at the acoustic resonance $f_1 \approx f_0$. With an increase in h, additional resonant peaks appear for $f_n = f_0/n$ (where n = 2,3,4 ...

is an integer) with amplitudes u_2 , u_3 , u_4 , etc., corresponding to the generation of the second, third, and higher voltage harmonics. We emphasize that the frequency of the generated voltage at each peak is equal to f_0 .

- d) With an increase in h, the resonance frequency may shift and the shape of u vs f may be distorted, or hysteresis may appear in the frequency response as shown in Figure 7d.
- e) The nonlinearity can lead to distortion of the voltage pulse generated by the structure with an increase in the amplitude of the excitation magnetic field pulse.

In the case of converse NLME, the nonlinearity also manifests similar to direct-NLME.

4.2 Nonlinear direct ME effects

This section is on studies of direct NLME effects when the composites are excited by an AC magnetic field and the voltage generated by the PE layer of the structure is measured.

4.2.1 Harmonic generation in a bipolar magnetic field

The nonlinear ME effect was first observed in a NZFO–PZT heterostructure under a low-frequency magnetic field modulation [35,68]. The sample contained alternating layers of PZT and NZFO, 18 μ m thick each, and was fabricated by laminating and sintering films synthesized by the tape casting method. Ag-electrodes were deposited on the surface of the multilayer sample and then it was poled in E=30 kV/cm. The sample was subjected to an in-plane magnetic field with an amplitude $H_{AC}=0.01-1$ kOe and a frequency f=1 mHz – 10 Hz. The dependences of the ME voltage u(t) on time were recorded, and then the frequency spectra were obtained by the Fourier transform. At low fields $H_{AC}<0.1$ kOe, ME voltage with at double the applied frequency (Fig. 8a) was recorded. At high fields, $H_{AC}\sim 1$ kOe, the ME voltage shape was distorted and up to 10 even harmonics appeared in the voltage versus frequency spectrum (Fig. 8b). The generation of harmonics was attributed to nonlinear dependence of $\lambda(H)$. Distortion of the ME voltage waveform was explained by saturation of the magnetostriction and finite conductivity of the PZT layers.

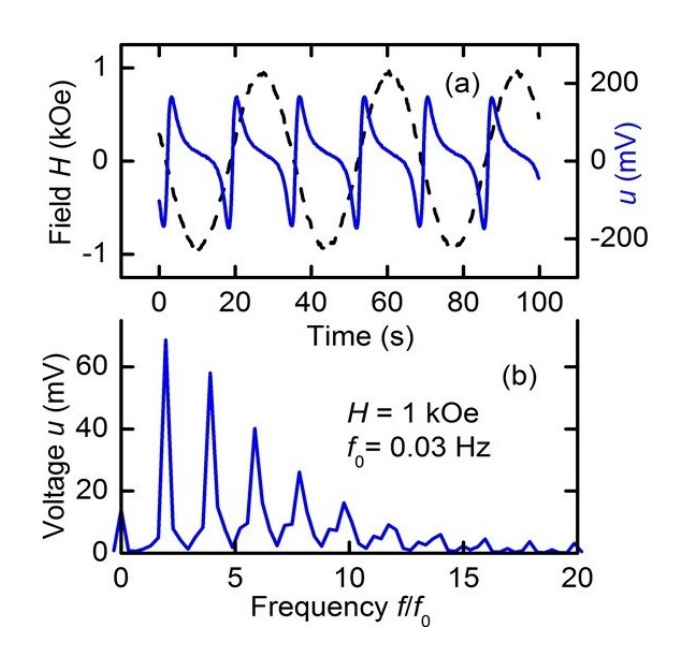


Fig. 8 Harmonic generation in the NZFO-PZT structure with bipolar field modulation: (a) is the dependence of the magnetic field H and ME voltage u on time, (b) is the frequency spectrum of the ME voltage.

Harmonic generation under bipolar field modulation in the absence of a bias magnetic field (H=0) was also observed in a multilayer containing Metglas layers between ferroelectric layers with Mn-doped PMN-PT fibers [69]. The sample was excited by an AC field with 0.1 < f < 40 kHz and an amplitude up to 9 Oe. For f_0 =1 kHz and with an increase in H_{AC} , distortion of the ME voltage and generation of even and odd voltage harmonics with frequencies f=2, 3, 4, and 5 kHz were observed. The distortion of the ME voltage waveform and generation of harmonics were also explained by the nonlinear dependence of Metglas magnetostriction and ohmic losses in Metglas.

Similar nonlinear ME effects were observed under bipolar field modulation in bulk composites [70]. A disk-shaped sample containing PZT and NiFe_{1.9}Co_{0.02}O₄ ferrite was excited by a bipolar field at 100 Hz and amplitudes up to 3 kOe applied parallel or perpendicular to the axis. The nonlinearity of magnetostriction led to doubling of the frequency of generated ME voltage and distortion of its shape.

4.2.2 Bias magnetic field influence on harmonics generation

The influence of a bias field H_{dc} on the generation of harmonics in the ME voltage in composites was reported in Ref. [71]. A PZT/Metglas sample was placed in a coil that created H_{dc} =0-100 Oe and an AC field $h\cos(2\pi ft)$ with a f =20 Hz - 2 kHz. For H_{dc} = 0, doubling of ME voltage frequency was observed (Fig. 9). It was shown that by changing H_{dc} one can control the frequency doubling efficiency. At $H_{dc}\approx$ 62 Oe, corresponding to the maximum of the piezomagnetic coefficient $\partial\lambda/\partial H$, the second harmonic vanished. The generation of the second harmonic was due to nonlinearity of Metglas magnetostriction.

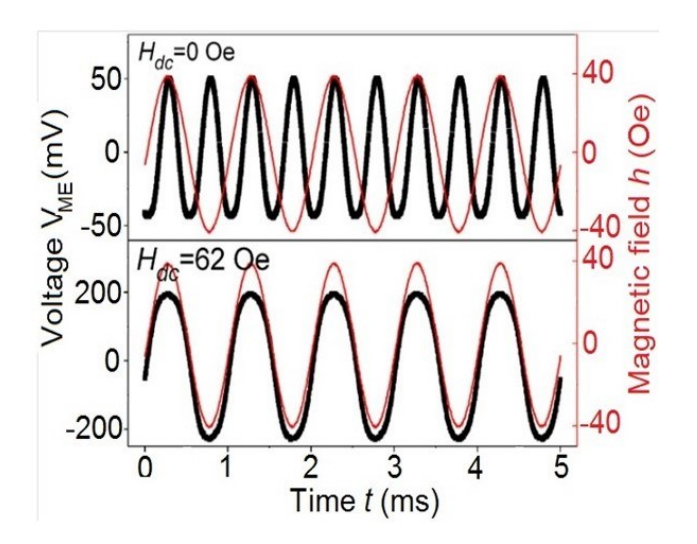


Fig. 9. Waveforms of alternative field h(t) and ME voltage $V_{\text{ME}}(t)$ in PZT/Metglas bilayer for bias fields H_{dc} =0 Oe and H_{dc} =62 Oe [Reproduced with permission from authors: Ref.71:J. Ma, Z. Li, Y. Lin, C.-W. Nan, A novel frequency multiplier based on magnetoelectric laminate, J. Mag. Magn. Mater. **323**, 101-103 (2011).].

Similar studies of the influence of bias magnetic field on the efficiency of second harmonic generation were carried out on Metglas-PZT and Metglas-PMN-PT layered samples [72,73]. A nonlinear ME coefficient was introduced $\alpha_E^{NL} = e/H_{ac}^2 = u/(a_p H_{ac}^2)$ with the dimension V/(cm·Oe²), where u is the amplitude of the second harmonic, a_p is the thickness of the piezoe-lectric layer. It was shown that dependence of $\alpha_E^{NL}(H)$ on H was determined by the dependence

of the H derivative of the piezomagnetic coefficient. The nonlinear ME coefficient was maximum at H = 0 and vanished in a field $H \approx 9$ Oe, at which the linear ME effect was maximum.

4.2.3 Generation of voltage harmonics under resonance conditions

The effect was first observed [74] in a Metglas-PZT bilayer sample. An in-plane bias field H = 0–12.6 Oe and an AC field with an amplitude up to h = 35 Oe and f = 0–20 KHz were applied. A peak in the ME voltage was observed at the bending resonance frequency of $f_r = 3.66$ kHz. As the frequency f of the excitation AC field was varied and for $f = f_n = (1/n)f_r$ (where n = 1,2,3...) the ME voltage showed additional peaks in u. It was found that the frequency of these voltage peaks was always equal to f_r . It was shown that when $n = f_r$, i.e., frequency doubling, tripling, etc., encountered in the ME response, resulted in a peak in the amplitude of u with a frequency f_r .

The resonant frequency doubling effect was studied in more detail in Ref. [75]. A PZT-bimorph-Metglas fixed at one end was excited by a field with f = 0-1 kHz and an amplitude up to h=20 Oe (Fig. 10). The bending resonance frequency was $f_0 = 695$ Hz. With H=18 Oe and when scanning the frequency of the field f, it was found that amplitude of u increased to a peak value at $f=f_0$. But with H=0, however, u showed a peak value with a frequency f_0 for $f=f_0/2$ and

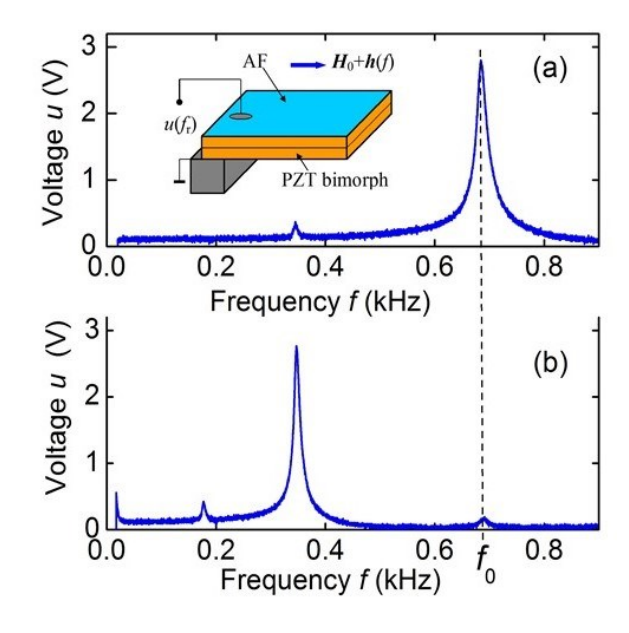


Fig. 10 Frequency doubling effect in PZT-bimorph/Metglas structure. (a) For H=18 Oe and h=20 Oe ME voltage shows a peak at f_0 . (b) For H=0 and h=20 Oe applied at half the resonance frequency $f_0/2$, the structure produces a ME voltage at f_0 .

this effect vanished at H=18 Oe. It was shown that shape of the field dependence of second harmonic amplitude coincides with H dependence of the nonlinear piezomagnetic coefficient $u_2(H) \sim \lambda^{(2)}(H)$, as predicted by the theory. Maximum value of the NLME coefficient under resonance conditions reached 0.48 V/(cm·Oe²), i.e., by a factor of 10^3 higher than under non-resonance conditions.

The frequency doubling in structures containing a PZT layer and FM layers of materials with very different saturation magnetostriction λ_S and saturation fields H_S was studied using layers of Metglas, Ni, and permendur (Co_{0.49}Fe_{0.49}V_{0.02}) [58,76]. For all of these composites, the dependence of the second harmonic amplitude on the field completely repeated the field dependence of the nonlinear piezomagnetic coefficient $u_2(H) \sim \lambda^{(2)}(H)$ and amplitude of the second harmonic depends quadratically on the amplitude of excitation magnetic field $u_2 \sim h^2$, in accordance with theory. The maximum resonant frequency doubling efficiency of ~4.5 V/(cm·Oe²) was reported in composites with Metglas, which has one of the highest nonlinear piezomagnetic modulus.

The second harmonic generation was observed in permendur-PZT upon excitation by magnetic field at a frequency equal to half the resonant one [77]. It was shown that amplitude of the harmonic increases quadratically with increasing the modulating field. It was shown in Ref.[78], that competition between quadratic magnetostriction and linear piezomagnetic effect leads to distortion of the second harmonic waveform in composites; a coefficient of nonlinear distortion was introduced which made it possible to quantitatively characterize generation of harmonics.

Resonant effects of frequency doubling in the flexible Metglas-P(VDF-TrFE) composite were reported at the frequencies of bending modes (~200 - 412 Hz) and longitudinal (~25 kHz) vibrations modes [79,80]. Generation of the 2nd and 3rd voltage harmonics was observed in two modes:

(a) when the sample was excited by h with $f = (1/n) f_r$ (n=2.3) and ME voltage u was recorded at f_r ; (b) upon excitation of the structure by h at f_r and voltage peaks were observed at frequencies $f = nf_r$ (n=2.3). In all cases, H dependence of the second harmonic amplitude repeated the field dependence of the nonlinear piezomagnetic coefficient $u_2(H) \sim \lambda^{(2)}(H)$, amplitude of the second harmonic depended quadratically on the amplitude of excitation field. Maximum value of the nonlinear ME coefficient in the structure reached 0.24 V/(cm·Oe²).

Nonlinear resonant effects were observed in a structure containing a 50 µm thick YIG $(Y_3Fe_5O_{12})$ ferrite film grown by liquid-phase epitaxy on a 310 µm thick dielectric substrate and a quartz plate [81]. The structure was excited by h at a frequency $f_0/2 \approx 64$ kHz (where f_0 is the resonant frequency of planar oscillations of the structure) and the voltage at the resonant frequency was recorded. Despite the small magnetostriction of YIG, $\lambda_S \approx 2.1 \cdot 10^{-6}$, due to high quality factor of the structure $Q\approx 2200$ in the absence of a bias field, H=0, the second harmonic generation efficiency $\alpha_E^{(2)} = 0.73$ V/(Oe²cm) was obtained, higher than in Ni-PZT structures.

The non-resonant and resonant generation of voltage harmonics in the Metglas-Langatate structure was studied at high excitation field amplitudes comparable to the bias $h\sim H$ [59]. It was shown

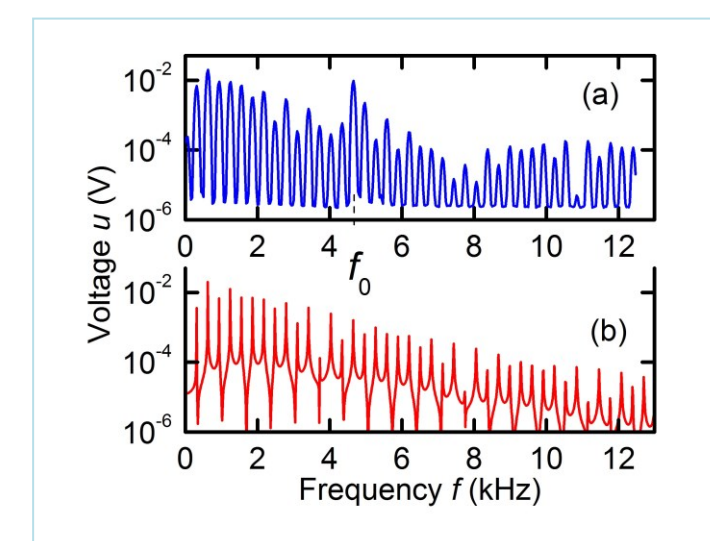


Fig. 11 Frequency spectrum of ME voltage under ME harmonics generation in Metglas-languatate composite: (a) experiment, (b) theory.

that at fields smaller than the saturation field of magnetostriction H_S , the amplitude of the n-th harmonic is proportional to the n-th derivative of magnetostriction with respect to the field and exhibits a power-law dependence

$$u_n(H) \sim \lambda^{(n)}(H)h^n$$
.

At high amplitudes of h, generation of up to $\sim 10^2$ voltage harmonics was observed (Fig. 11), which indicates a high

nonlinearity of ME effects in heterostructures. A method is proposed for calculating voltage harmonic amplitudes at high amplitudes of the excitation field, which consists in finding the time dependence of the ME voltage using the shape of the excitation field and field dependence of magnetostriction $\lambda(H)$ and the subsequent application of the Fourier transform.

Resonant generation of harmonics was predicted [82] and observed [83] in a ring-type FM-PE heterostructure. The structure was a PZT ring, 18 mm in diameter, with a 27 μ m thick Metglas layer glued on its inner surface. A circumferential excitation field h and a permanent bias field H were produced by electromagnetic coils wound on the ring. Due to the absence of demagnetization effects in the ring, the ME nonlinearity was observed at lower fields h, compared to the planar structure.

Figure 12 shows the dependence of ME voltage u on the excitation field frequency f. At small h < 0.1 Oe, a linear ME effect was observed in the structure. The dependence contained only one

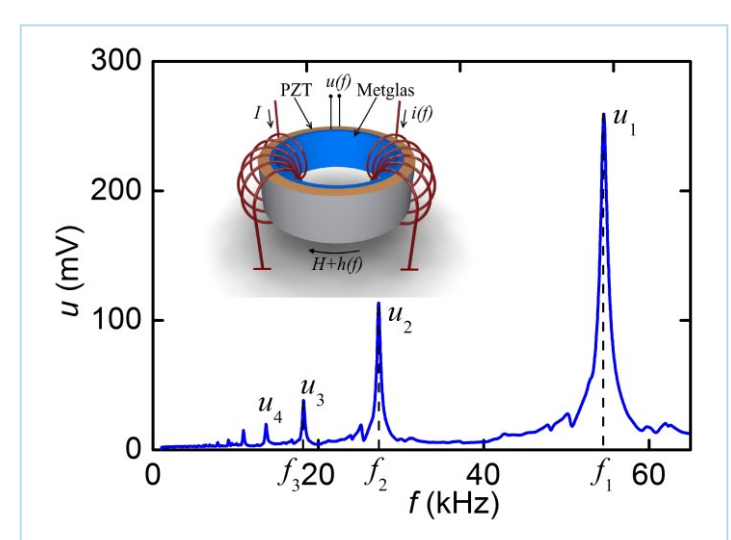


Fig. 12 Dependence of ME voltage *u* on the excitation field frequency *f* for the Metglas-PZT ring-type heterostructure.

resonant peak with a frequency of radial vibrations of the ring f_1 =54.2 kHz. As the field increased above $h\approx0.5$ Oe, several peaks appeared on the characteristic at the excitation frequencies $f_n = f_1/n$ (where n=2, 3, 4, ...) with amplitudes of u_2 , u_3 , and u_4 , respectively. The frequency of the generated ME voltage for all peaks was equal to the frequency of the main resonance of the structure f_1 .

Thus, a field with frequency f_2 generated a voltage of double frequency, a field with frequency f_3 generated a voltage of triple frequency, etc. Amplitudes of the harmonics increased with increasing h as $u_n \sim h^n$, in accordance with the theory.

4.2.4 Generation of combination frequencies under resonance conditions

The frequency mixing effect in the ME structure was observed in the Metglas-PMN-PT and

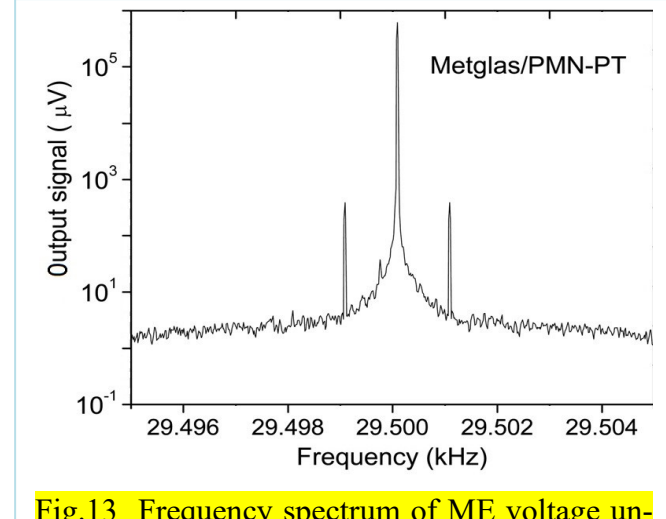


Fig.13 Frequency spectrum of ME voltage under resonant mixing of two magnetic fields with different frequencies in Metglas-PMN-PT [Reproduced with permission from authors: Ref.84]: L. Shen, M. Li, J. Gao, Y. Shen, J. F. Li, D. Viehland, X. Zhuang, C. Lam, C. Cordier, S. Saez, C. Dolabdjian, Magnetoelectric nonlinearity in magnetoelectric laminate sensors. J. Appl. Phys. 110(11), 114510 (2011).

Metglas-PZT composites [84,85]. The samples were magnetized by a bias magnetic field H and simultaneously excited by two ac magnetic fields: an H_{ins} at f_0 equal to the acoustic resonance frequency and a low-frequency field H_{AC} at $f_1 = 1$ Hz and an amplitude of 10 nT. It is shown, that the nonlinearity of magnetostriction leads to the appearance of components with combination frequencies $f_0 \pm f_1$ in the frequency spectrum of the output voltage (see Fig.13). To estimate the efficiency of frequency mixing, a nonlinear **ME** coefficient $\alpha_E^{nonl} = E/(H_{ins}H_{AC})$ with units of

 $V/(cm\cdot Oe^2)$ was introduced in. It was established that the amplitude of the side harmonic depends on H. For the Metglas-PMN-PT sample, the maximum coefficient was 25.3 $V/(cm\cdot Oe^2)$ for H=0.

The nonlinear ME effect of mixing the frequencies of magnetic fields was studied in more detail in Ref. [86]. We used a PZT-bimorph - Metglas heterostructure with bending mode frequency of f_0 =0.695 kHz. The sample was magnetized by a bias field H and excited by two harmonic fields $h_1 \cos(2\pi f_1 t)$ and $h_2 \cos(2\pi f_2 t)$. Figure 14 shows mixing of the frequencies of the two fields when scanning the frequency f_1 of the first field and different frequencies f_2 of the second field at h_1 = h_2 =10 Oe and H=0. When ME effect was excited by a single field h_1 (f_2 =0)

with a frequency $f_1 \approx 0.35$ kHz, the composite generated a voltage with a resonance frequency, i.e.,

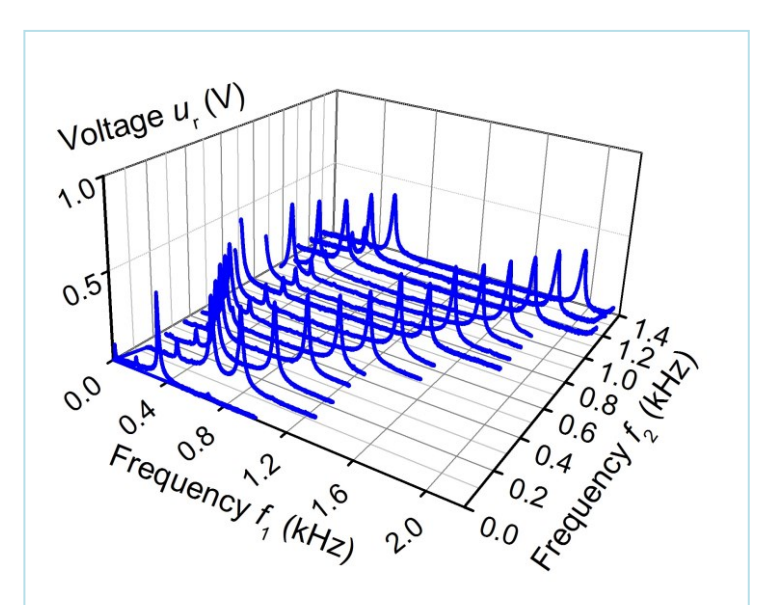


Fig. 14 Dependence of the ME voltage u on the frequencies of the magnetic fields f_1 and f_2 when the fields are mixed in the PZT-bimorph - Metglas structure.

frequency doubling took place. When the second field was turned on, the peak near the frequency 0.35 KHz disappeared, but two peaks appeared near the frequencies satisfying the matching conditions

$$f_1 + f_2 = f_0$$
 and $f_1 - f_2 = f_0$. (22)

The separation between the peaks increased with increasing f_2 . At $f_2=f_0$ the frequency of the first peak went to zero and frequency doubling took

place. As f_2 increases, the separation between the peaks remained equal to $\Delta f = f_2 - f_1$, and they both shifted to the high-frequency region. The dependence of the voltage amplitude on H, as in the case of frequency doubling, repeated the field dependence of the nonlinear piezomagnetic coefficient $u(H) \sim \lambda^{(2)}(H)$. At a fixed field h_2 , the peak amplitudes first linearly increased with an increase in the field h_1 , and then saturated at $\sqrt{h_1 h_2} \approx H_S$, where H_S is the saturation field of the ferromagnetic layer. The frequency mixing efficiency reached $\sim 0.25 \text{ V/(cm·Oe}^2)$.

The effect of ME voltage generation at resonance frequency upon excitation by fields with different frequencies satisfying the phase-matching condition was also observed [58] in composites containing a PZT layer and FM layers made of materials with significantly different magnetostrictive characteristics: Metglas, Ni, and permendur. The frequency mixing efficiencies were ~3.2 V/(cm·Oe²) for Metglas, ~0.16 V/(cm·Oe²) for Ni, and ~0.08 V/(cm·Oe²) for permendur, respectively. In Ref. [78], the effect of frequency mixing was observed in a sample with layers of

Metglas and PVDF with an efficiency of ~30 mV/(cm·Oe²). The characteristics of combination frequency generation in all structures studied are well described by the theory.

4.2.5 Non-collinear excitation of nonlinear effects

Characteristics of NLME effect in the Metglas-PZT structure were studied under excitation with a field h directed perpendicular to the permanent field, $h \perp H$ [87]. A disk-shaped sample was used to eliminate the effect of demagnetization. The fields h and H were applied in the sample plane. In the non-resonant mode, for $f=f_0=5$ kHz and with an increase in h to 3 Oe, the generation of voltage harmonics at $f=nf_0$ and amplitudes u_n , where n=1,2,3,4... was observed. Figure 15 shows the dependence of the second harmonic amplitude u_2 on the permanent field H at $h \perp H$

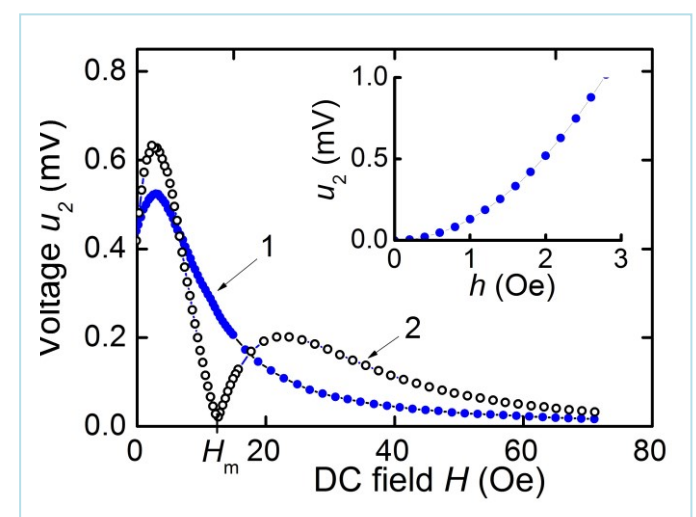


Fig. 15 Dependence of the amplitude of the second harmonic of the ME voltage u_2 in the Metglas-PZT composite on H for: $1 - h \perp H$ and 2 - h//H.

and, for comparison, at $h/\!/H$. When a nonlinear ME effect is excited by a transverse field, the dependence qualitatively differs from the traditional case. The harmonic amplitude u_2 decreases monotonically with increasing field. Theoretical analysis has shown that H dependence of u_2 in the case of transverse excitation has the form $u_2(H) \sim \left[\lambda^{(1)}(H)/H\right]h^2$. The main contribution to the second harmonic gener-

ation is made by the excitation geometry and the field dependence of the linear coefficient [88], rather than the nonlinearity of the magnetostriction. The inset of Fig. 15 shows the quadratic dependence of $u_2(h)$ on the field amplitude, which is in good agreement with the theory.

In Ref. [89], NLME effects were observed in a Metglas-PZT disk structure placed in a tangential bias field H upon excitation by a rotating magnetic field h in the disk plane. The nonlinearity of λ also led to the generation of voltage harmonics. The harmonics had a specific field dependence of the amplitude of H and h, different from the case of structure excitation by a longitudinal or transverse field. A theory is developed that describes well the characteristics of the NLME effect in the limiting cases of weak, h < H, and strong, h > H, excitation fields.

4.2.6 Excitation of nonlinear ME effect by magnetic noise

The nonlinearity of ME effects is clearly manifested when the composites are excited by a magnetic field with a noise spectrum [90]. The ME voltage spectra were studied in a symmetrical three-layer Metglas-languatate-Metglas structure. The sample was non-resonantly excited by a magnetic field a rectangular noise spectrum $h(f_N)$ with a central frequency $f_N = 0.5-10$ kHz and a

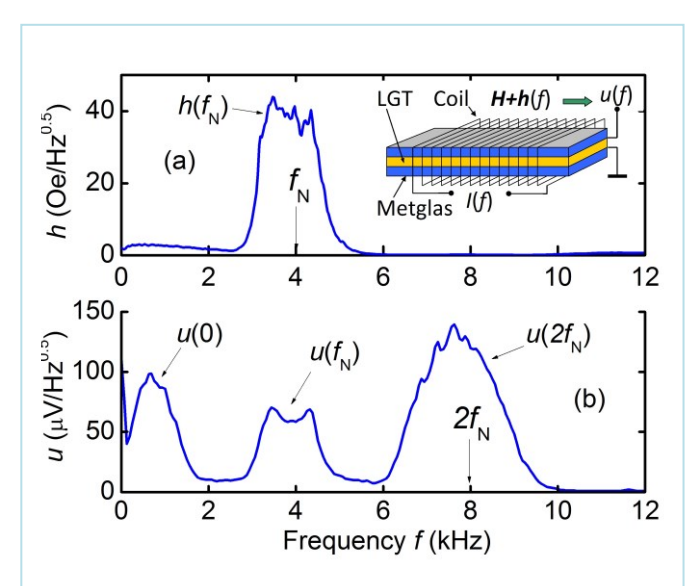


Fig. 16 Excitation of the Metglas-langutate structure by a magnetic field with a noise spectrum: (a) frequency spectrum of the magnetic field, (b) frequency spectrum of the generated ME voltage.

width $\Delta f \approx 0.5$ –2 kHz (Fig.16a). It is found that magnetic noise leads to linear generation of electrical noise $u(f_N)$ with center frequency of f_N and nonlinear generation of electrical noise u(0) close to zero frequency, and noise $u(2f_N)$ in the region of doubled frequencies $2f_N$, which is shown in Fig. 16b.

An even richer ME voltage spectrum was observed [91] when a three-layer Metglas-Langatate-Metglas structure was excited simultaneously by a harmonic magnetic field with a frequency f_p and magnetic noise

with a rectangular spectrum and central frequency of f_N . In this case, peaks with frequencies $f_p \pm f_N$ and $f_p \pm 2f_N$ and noise pedestals at the bases of the peaks additionally appeared in the

voltage spectrum. The shape of the spectral density peaks of linear and nonlinear voltages, as well as the dependences of the ME voltage on the bias field H and the amplitude h of the excitation fields, are well explained by the theory of nonresonant mixing of magnetic fields in ME composites with a nonlinear dependence of magnetostriction on the field.

4.2.7 Enhancement of nonlinear ME effect due to nonlinearity of magnetization

In addition to nonlinearity of $\lambda(H)$, the nonlinear dependence of the ferromagnet magnetization on the field M(H) also contributes to the NLME effect (see Fig. 2b) [92]. When the composite is excited by an ac field $h_1\cos(2\pi ft)$, the nonlinearity of M(H) leads to the generation of magnetic field in the FM layer at 2f and amplitude $h_2 = (1/2)(\mu^{(1)}/\mu)h^2$, where $\mu(H)$ is the magnetic permeability and $\mu^{(1)}(H) = \partial \mu/\partial H|_H$ is its derivative with respect to the field. In fact, the sample is excited by combination of two fields $h = h_1 \cos(2\pi ft) + h_2 \cos(4\pi ft)$. Field h_1 excites the second harmonic in the nonlinear mode, and field h_2 in the linear mode. The amplitude of the second harmonic is given by

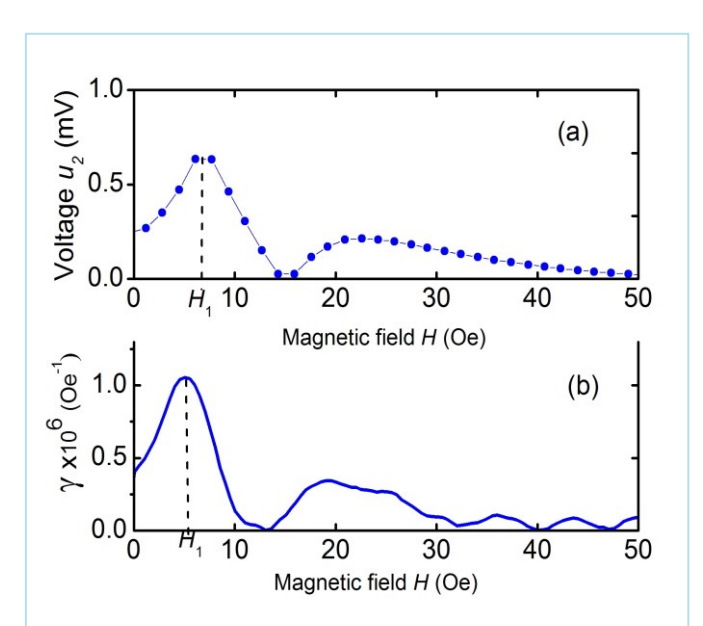


Fig. 17 Magnetic field H dependence of (a) second harmonic of ME voltage u_2 , and (b) renormalized piezomagnetic coefficient γ .

$$u_{2} = \frac{1}{4} d_{31} \left[\lambda^{(2)} + \frac{2\mu^{(1)}}{\mu} \lambda^{(1)} \right] h_{1}^{2}.$$
(23)

Thus, the nonlinearity of M(H) leads to a renormalization of the nonlinear piezomagnetic coefficient. Figure 17 shows measured field dependence of the second harmonic amplitude u_2 for a Metglas-PZT composite and field dependence of the renormalized piezomagnetic coefficient $\gamma(H)$, calculated using Eq.(18) and measured dependences $\lambda(H)$ and M(H). It can be

seen that the two profiles track each other and are in good qualitative agreement. Taking into account the nonlinearity of M(H) makes it possible to explain the appearance of the maximum of the second harmonic in weak fields, which is observed in experiments.

4.2.8 Static deformation of ferromagnet in alternating field

The theory for NLME effects predicts that the nonlinearity of λ should lead to static deformation of composite structures (see Eq.6a) in an alternating field. The effect was reported in plates of FeCo and Ni placed in H=0-2 kOe and h with a frequency of 50 Hz [93]. The static deformation

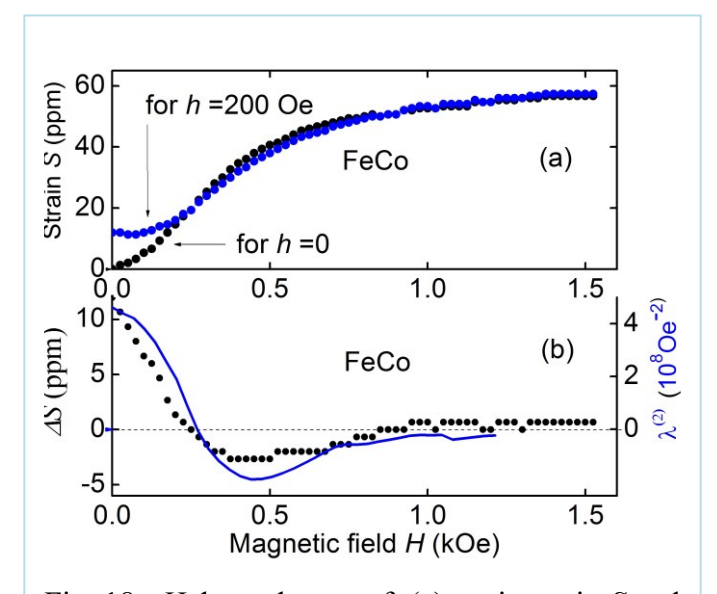


Fig. 18. H dependences of: (a) static strain S and (b) change in strain ΔS under the action of an AC field h in a FeCo ferromagnet plate.

of the samples was recorded using a strain gauge. Figure 18(a) shows the dependence of the static strain S of a FeCo plate on H and for h=0 and 200 Oe. Figure 18(b) shows the change in the plate deformation $\Delta S = S(H,h) - S(H,h=0)$ under the action of the alternating field. For H=0, the FeCo plate was additionally stretched (and the Ni plate was compressed). Value of the deformation caused by h reached $\sim 50\%$ of the saturation magnetostriction λ_S . The

field dependence of the deformation repeated the field dependence of the nonlinear piezomagnetic coefficient $\Delta S \sim \lambda^{(2)}(H)$, in agreement with the theory

4.2.9 Suppression of hysteresis in nonlinear ME effects

The dependence of the magnetostriction of most materials on H has a hysteresis. The value of the coercive field is $H_c < 1$ Oe for amorphous alloys and reaches $H_c \sim 200$ Oe for Co and Terfenol-D. This leads to a hysteresis phenomenon in the H dependence of the characteristics of NLME

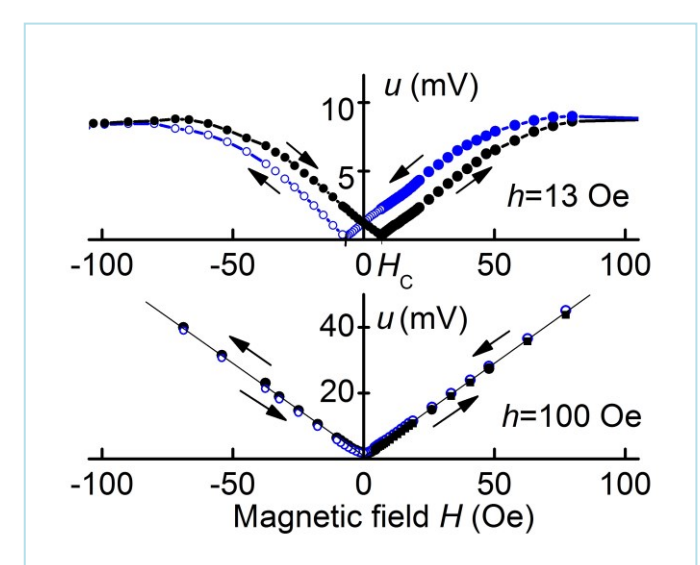


Fig. 19 Dependences of ME voltage u vs. H in the Ni-PZT structure for h=13 Oe and h=100 Oe.

effects. Suppression of hysteresis in the H dependences of amplitudes of the first and third ME voltage harmonics were observed in a Ni-PZT composite [94,95]. The coercive field H_c decreased from 21 Oe to \sim 0.4 Oe with an increase in the amplitude of h from 1 Oe to 100 Oe (see Fig. 19). Calculations have shown that the hysteresis is suppressed due to a decrease in the relative influence of H on the asymmetry of the magnetostriction loop of the Ni layer with

an increase in the amplitude of h.

4.2.10 Excitation of nonlinear ME effects in composites by a current through the magnetic layer

Manifestation of NLME effects as generation of voltage harmonics was observed in a Metglas-PZT bilayer under a current through the Metglas layer and subjected to H (Fig. 20) [96,97]. The

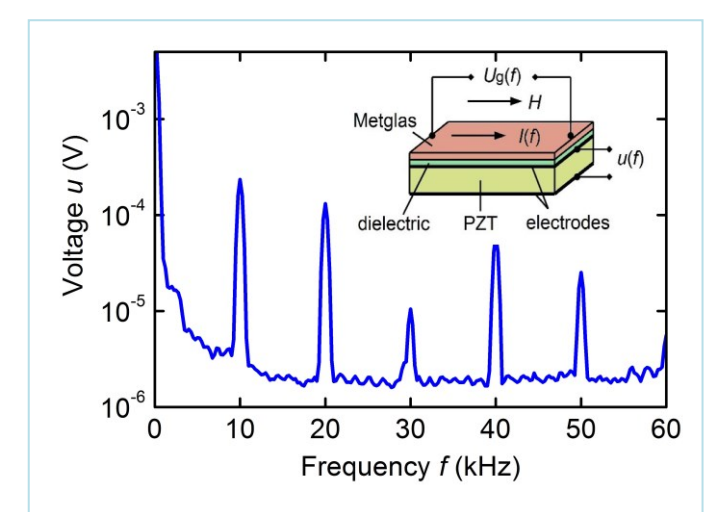


Fig. 20 Frequency spectrum of the ME voltage u(f) upon excitation of the NLME effect in a Metglas-PZT bilayer by current I at 10 kHz flowing through the Metglas layer.

current creates an excitation field h in the FM layer that is inhomogeneous along its thickness and is directed perpendicularly to H. With this method of excitation, demagnetization effects do not affect the magnitude of the excitation field, which results in significant enhancement in the efficiency of voltage harmonics generation compared to excitation by a coil. The efficiency of nonresonant second harmonic generation at longitudinal resonance of the

sample at f_0 =46 kHz was ~0.08 V/(cm·Oe²) for I=200 mA and H=0 The amplitude of the second voltage harmonic decreased with increasing H as $u_2 \sim 1/H$, as it should be when the NLME effect is excited by a transverse magnetic field [87].

4.3 Nonlinear converse ME effects

In this section, we consider studies on nonlinear converse ME effects due to excitation of FM-PE composites with an ac electric field and measuring changes in the magnetization of the FM layer.

4.3.1 Harmonic generation and field mixing at converse NLME effect

The converse NLME effect was observed in a planar bilayer of Metglas-PZT comprizing a 20 μ m thick FM layer and 0.2 mm thick PZT layer [98]. The sample was placed in a tangential magnetic field H = 0-100 Oe, and an AC electric field of amplitude e = 0-250 V/cm and f = 0-200

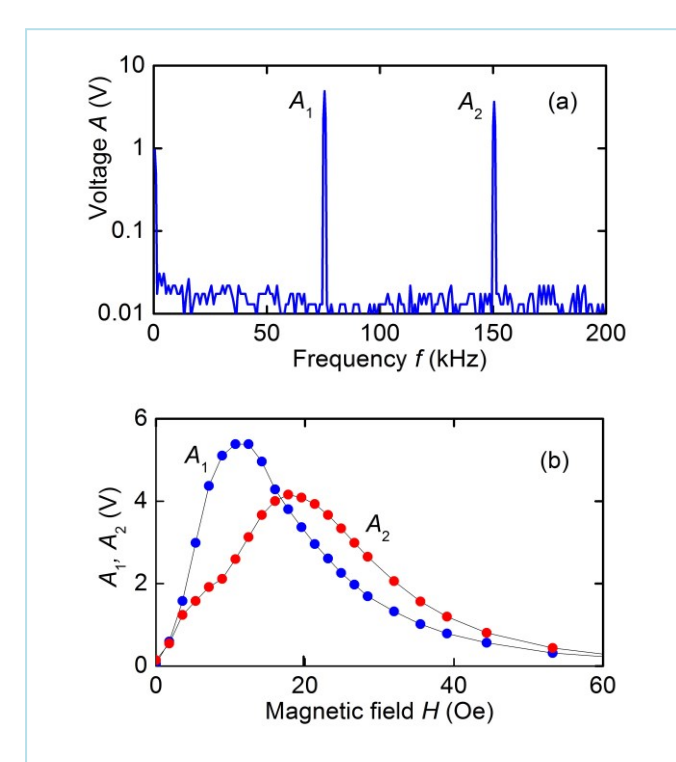


Fig. 21 Nonlinear converse ME effect in the Metglas-PZT structure: (a) ME voltage frequency spectrum, (b) dependence of the amplitudes of the first and second voltage harmonics A_1 and A_2 on the bias field H.

kHz was applied to the piezoelectric layer. Changes in the magnetization of the FM layer were recorded using a pickup coil. Under excitation at the longitudinal acoustic resonance frequency of 76 kHz, the first and second voltage harmonics were observed in the pickup coil voltage spectrum (Fig. 21a). The amplitudes of the first and second harmonics depended on H (Fig. 21b) and increased linearly and quadratically, respectively, with increasing excitation field e. The linear and nonlinear field conversion coefficients were $\alpha_B^{(1)} \approx 5.5$ G/(V/cm) and $\alpha_B^{(2)} \approx 1.9 \cdot 10^{-2}$ G·cm²/V². It was shown that

NLME effects in the bilayer arose due to nonlinear dependence of the Metglas layer magnetization on the deformation created by the PZT layer. A theoretical model was developed to explain the field and amplitude characteristics of the nonlinear converse ME effect.

4.3.2 Harmonic generation and field mixing in structure with electrostrictor

Harmonic generation under the converse NLME effect was found in a planar structure containing layers of Metglas and an electrostrictive (ES) single-crystal PMN-PN [99]. The ES layer had a permittivity $\varepsilon \approx 6.10^3$ and an electrostriction coefficient $R \approx 2.65 \cdot 10^{-16}$ m²/V². The sample was excited by e at $f = f_0/2$ and a change in magnetization at resonance frequency $f_0 \approx 72$ kHz was recorded using a pickup coil. For the linear field conversion, a coefficient of $\alpha_B^{(1)} \approx 0.1$ G/(V/cm) was obtained and for a nonlinear one $\alpha_B^{(2)} \approx 3.10^{-6}$ G/(V²cm²).

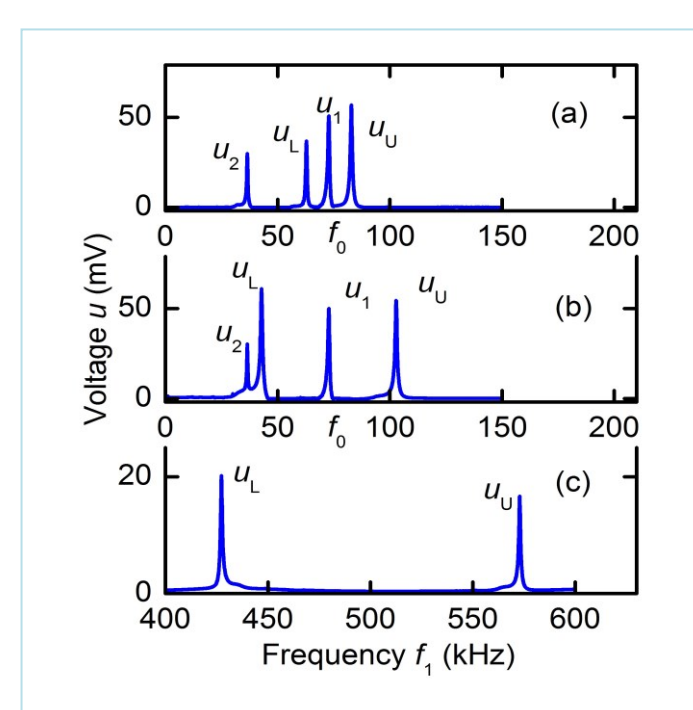


Fig. 22 Frequency f_1 dependences of the ME voltage u measured in a pickup coil enclosing a Metglas-PMN-PT bilayer. The frequency of the second excitation electric field was set at f_2 :

(a) 10 kHz, (b) 30 kHz and (c) 500 kHz.

When the sample was excited by two electric fields with frequencies f_1 and f_2 , the generation of magnetization at combination frequencies was observed.

Figure 22 shows the dependences of u from the pickup coil on f_1 for fixed frequencies f_2 =10, 30 and 500 kHz. The characteristics show peaks near f_0 /2 and f_0 , as in the case of doubling the frequency. In addition peaks with frequencies f_L and f_U are seen, satisfying the conditions of frequency matching

$$\left| f_U \mp f_L \right| = f_0. \tag{24}$$

Nonlinear ME effects in FM-ES structures arise due to nonlinear dependence of the deformation in the ES layer, which has the form $\eta = R \cdot E^2$, where R is the constant coefficient [100,101]. The direct NLME effect was not observed in the bilyer with an electrostrictor. A theory was developed to explain the field and amplitude characteristics of the frequency doubling and frequency mixing effects in the FM-ES bilayer.

4.3.3 Mixing of frequencies of electric and magnetic fields

The frequency mixing of magnetic and electric fields in a disk shaped Metglas-PZT composite was demonstrated in Ref.[102]. The sample was excited in a non-resonant mode by a magnetic field with a frequency $f_{\rm m}$ created by a coil and an electric field with a frequency $f_{\rm e}$. The change in the magnetization was recorded using a second coil. In the frequency spectrum of the voltage generated by the receiving coil, in addition to the linear components and components of frequencies $2f_{\rm m}$ and $2f_{\rm e}$, there were harmonics with the combination frequencies $f_{\rm e} \pm f_{\rm m}$. The nonlinear converse ME effect coefficient was $4.6\cdot10^{-6}$ G/(V²/cm²), and the coefficient of nonlinear mixing of magnetic and electric fields was $\alpha_B^{(2)} \approx \sim 1\cdot10^{-2}$ G·cm/(Oe·V). It is shown that the field mixing is due to the nonlinearity of the Metglas layer inverse magnetostriction. A theory was presented that describes the mixing of magnetic and electric field frequencies in the composite.

In [103], the resonant frequency mixing was observed in a 200 μ m thick PZT layer with electrodes with one side bonded to a 40 μ m thick Metglas film and the other side to a 40 μ m thick PZT film. When the sample was excited by a magnetic field $h(f_1)$ and an electric field $e(f_2)$ was applied to the PZT film, the PZT layer generated a voltage with combination frequencies.

4.3.4 Parametric generation of sub-harmonics of magnetization

A typical phenomenon for nonlinear systems is parametric generation of sub-harmonics. In the case of converse ME effect, subharmonic generation was observed in a Metglas-PZT disk resonator [104]. The resonator with mutually perpendicular coils as in Fig.23a was magnetized with a

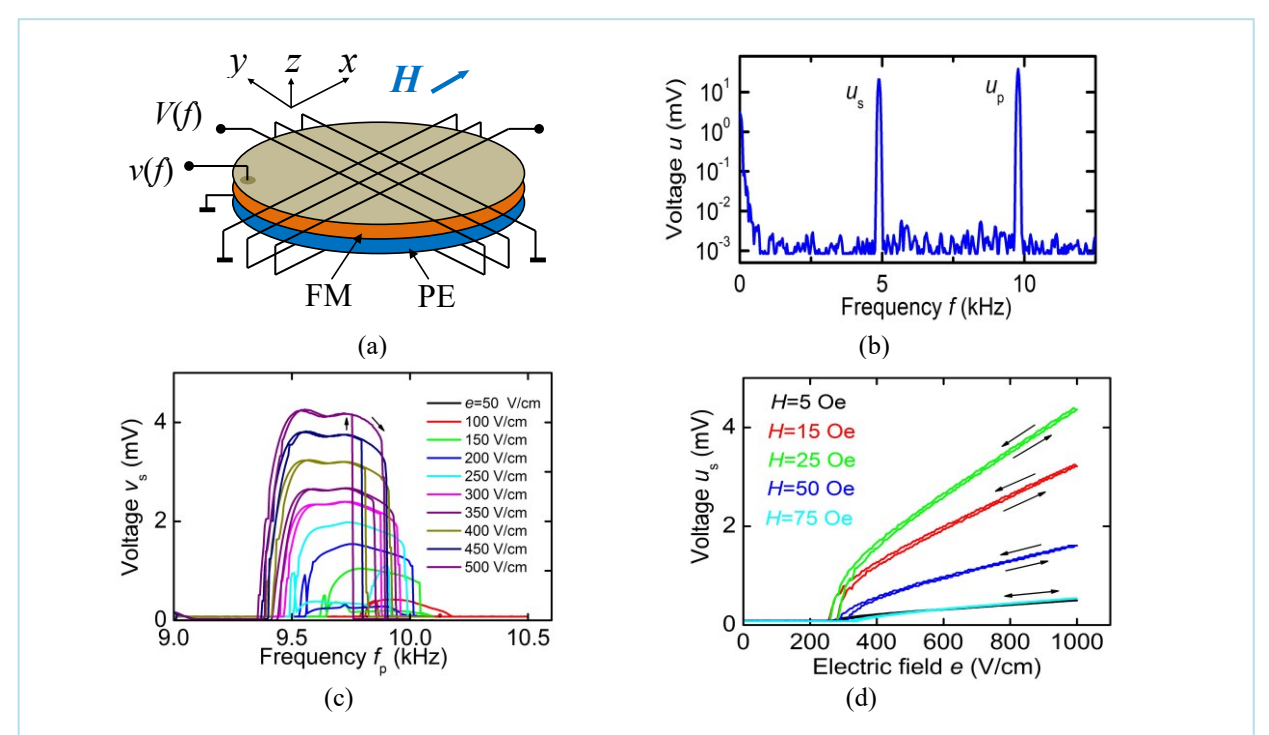


Fig. 23 Generation of sub-harmonics in a Metglas-PZT disk resonator: (a) resonator setup, (b) frequency spectrum of the ME voltage, (c) dependence of the sub-harmonic amplitude on the pump frequency f_p , (d) dependence of the sub-harmonic amplitude on the excitation field amplitude e.

tangential field H=0-100 Oe. The resonator was excited with h=5 Oe at f= 9-10 kHz applied to a coil or with e=500 V/cm, applied to the PZT layer.

When a threshold field was exceeded, the sub-harmonic generation at f/2 was observed by three different methods: at the direct ME effect, at the converse ME effect, and in the transformer mode. The sub-harmonic was generated in a limited frequency range and its amplitude depended nonlinearly on the pump amplitude and the bias magnetic field. A theory for parametric sub-harmonics generation in a multiferroic resonator was developed, that takes into account magnetoacoustic nonlinearity of the FM layer of the structure and excitation of acoustic resonances at frequencies near the pump and sub-harmonics. The theory qualitatively well describes characteristics of sub-harmonics in the composite.

4.3.5 Noise generation at converse ME effect

Stochastic noise generation was observed in a Metglas-PZT disk resonator under the converse ME effect [105]. The resonator was placed in a tangential field H = 0–100 Oe and excited by e = 330 V/cm at f = 2–10 kHz applied to the PZT layer. Changes in the magnetization of the resonator were recorded using a pickup coil. An increase in e above a threshold led to the generation of voltage harmonics and sub-harmonics with a discrete spectrum, which then acquired a stochastic form and turned into a continuous noise spectrum (Fig. 24). The spectral noise density hysteresically depended on e and nonmonotonically depended on e. A theory of parametric noise generation for converse ME effect was developed, which takes into account the magnetoacoustic nonlinearity of the FM resonator layer and qualitatively describes the experimental data.

4.3.6 Bistability in composite resonators

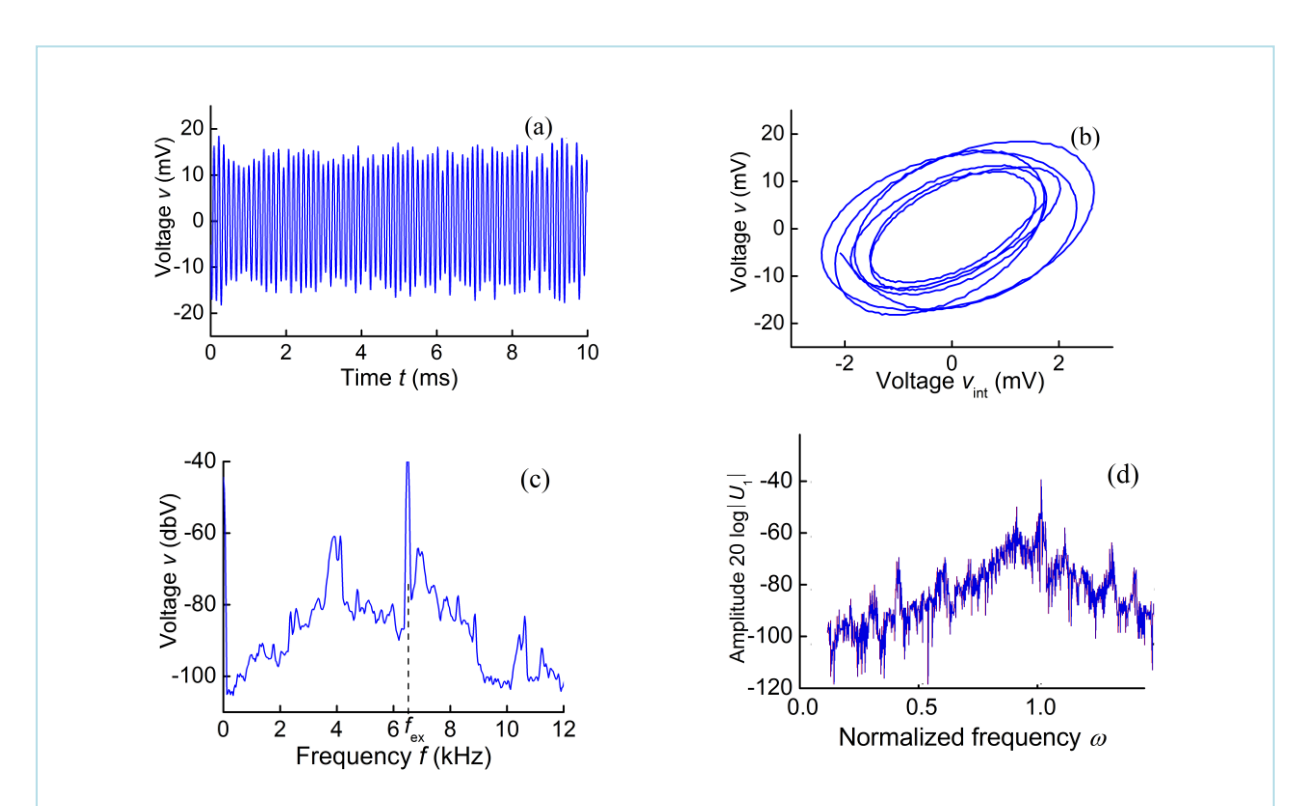


Fig. 24 Noise generation in Metglas-PZT resonator: (a) generated voltage, (b) phase portrait, (c) noise spectrum, (d) calculated noise spectrum.

Bistability, i.e. the existence of two stable states of a dynamic system at different levels of the excitation force is one of the important manifestations of nonlinearity. In composite resonators, bistability was apparently first reported in Ref.[106]. The authors used a FeGa-PZT microcantilever, 950 µm long, 200 µm wide, and 5 µm thick. Bending oscillations of the cantilever at a fre-

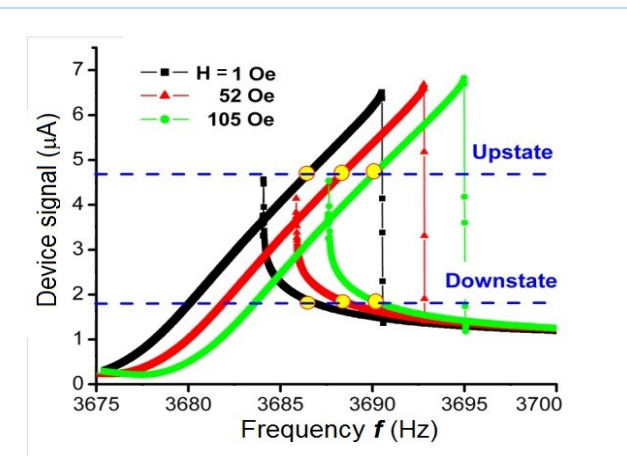


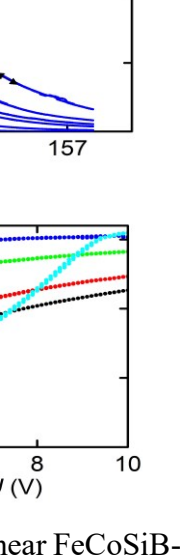
Fig. 25 Bistability loops in a nonlinear FeGa-PZT microcantilever at different values of a bias magnetic field H [106].

quency of 3.836 kHz were excited by an electric field applied to the PZT film.

The response of the structure was recorded by the change in the excitation current. In the absence of a bias magnetic field (*H*=0), with increasing voltage, distortion of the resonance line and an up-shift of the resonance frequency were observed (Fig.25). Shift of the frequency was explained by a change in the rigidity of the pi-

ezoelectric layer. When sweeping the frequency up and down, typical bistability loops were registered. When a field H = 0-105 Oe was applied to the cantilever, the resonator frequency was tuned and the shape of the loop changed due to changes in the rigidity of the system.

The bistability phenomenon was also observed in a FeCoSiB-AlN resonator, 25 mm x 2 mm in size and 150 μ m thick [107]. The resonator was excited by an electric field at a frequency of longitudinal acoustic oscillations $f_0 \approx 156$ kHz (Fig.26). The bistability loops were measured with a frequency sweep for a fixed excitation field amplitude e (Fig. 26 a) and with a change in the field amplitude e at a fixed frequency (Fig. 26b). Loops were observed both from the low frequency side and from the high frequency side of the resonance line. It was shown that the bistability arises due to nonmonotonic dependence of the resonance frequency on e. With increasing e, the frequency first decreased by ~ 0.7 kHz and then increased to the initial value. A model of dispersive bistability discussed in the work takes into account the Lorentz shape of the resonance line and the



f scan and (b)

field.

measured dependences of the frequency and transmission coefficient of the resonator on the excitation field. It is shown that the bistability in the resonator arises due to the nonlinearity of the ferroic order parameters of the FM layer.

In Refs. [108,109], the bistability was reported in a Metglas-PMN-PZT composite. The sample was magnetized by a field H and excited by an electric field at a longitudinal acoustic resonance frequency of ~40 kHz. The change in the magnetization was recorded using a coil. Distortion of the shape of resonance and a bistability loop were found under cyclic scanning of the field frequency near the resonance. At a constant frequency, the dependences of the output signal on H were measured at different excitation voltages, at which jumps in the output signal were found. The authors associated the occurrence of bistability with the nonlinearity of the FM layer, in particular, with a change in its rigidity under the action of magnetic field.

4.3.7 Parametric amplification in multiferroic composites

Parametric amplification of the ME effect in a composite resonator was reported in Ref. [110]. The authors used a FeGa-PZT microcantilever, 950 μ m long and 200 μ m wide. The cantilever was excited at the lowest bending vibration mode $f_0\approx3.55$ kHz by an ac magnetic field $h\approx0.28-27$ nT, and the voltage generated by the PZT layer was recorded. To parametrically amplify the output voltage, a pump voltage with at twice the frequency $f_p=2f_0$ and an amplitude V_p of up to 1.2 V was applied to the PZT layer electrodes. At low pump amplitudes, $V_p<0.1$ V, pumping did not affect the output voltage. As the voltage was increased to the threshold value $V_1\approx1.1$ V, amplitude of the signal increased exponentially and ME coefficient increased from $\alpha_E\approx33$ mV/(Oe cm) to 2 MV/(Oe cm). The quality factor of the resonator Q in this case increased from 3000 to ~35000 . The standard theory of parametric amplification was used to explain the results.

Parametric amplification was also observed in a Metglas-PZT disk resonator [111]. Acoustic oscillations in the resonator at a frequency of 3.08 kHz were excited and recorded using two crossed coils (see Fig.27). Pumping was carried out by an electric field with doubled frequency and amplitude up to e=500 V/cm, applied to the PZT layer. With increasing pumping, the oscillation amplitude increased as $u(e) \approx u_0 (1-e/e_{th})$. At a threshold pump amplitude $e_{th} \approx 300$ V/cm, an oscillation amplification factor of 22 dB was achieved. For pump fields $e > e_{th}$, the system

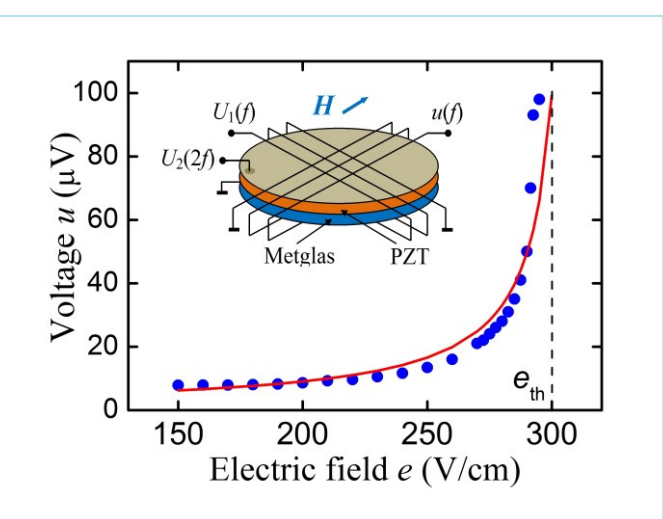


Fig. 27 Dependence of the ME coefficient on the pump voltage for parametric amplification of oscillations in a composite disk of Metglas-PZT. The solid line is the calculated values.

switched to the stationary generation regime. The authors explained this parametric amplification by a change in the stiffness of the structure under the action of a permanent electric field.

4.4 Nonlinear ME effects under pulsed excitation

NLME effects under pulsed excitations was first reported in Refs. [112,113]. A

multilayer NZFO-PZT composite with 20 μ m thick alternating layers of NFO and PZT was used. The sample was magnetized by a field H, and excited by pulses of magnetic field h(t) with a duration of $\tau \approx 1$ μ s and an amplitude of up to 150 Oe. The envelope and frequency spectrum of the generated electrical pulses were recorded. Distortion of the pulse shape due to nonlinearity of magnetostriction and excitation of acoustic vibrations of the structure were observed (Fig. 28). The shape of the composite response depended on the field H.

.

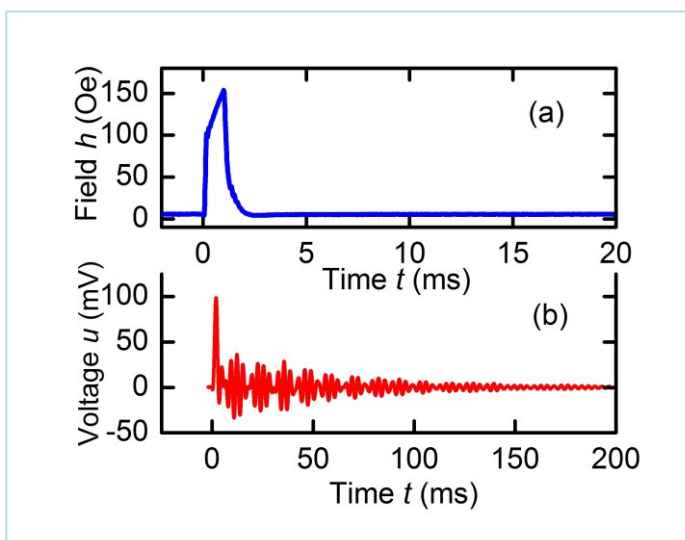


Fig. 28 ME response of the NZFO-PZT composite upon excitation by magnetic field pulses: a) field pulse, b) voltage pulse.

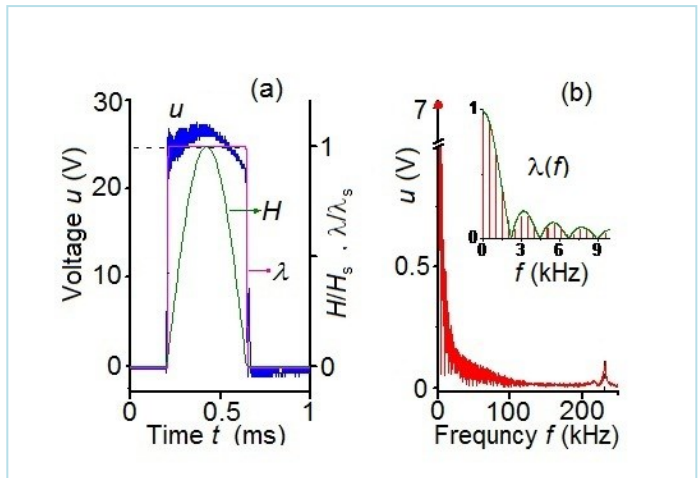


Fig. 29 ME response of the Co-PZT sample upon excitation by magnetic field pulses with an amplitude of up to 38 kOe: a) shape of the field H(t), strain $\lambda(t)$, and voltage u(t) pulses, b) frequency spectra of the strain $\lambda(t)$ and voltage u(t) pulses.

In Ref.[114], similar effects were observed when twoand three-layer Permendur-PZT and Ni-PZT composites were excited by a pulsed magnetic field in the form of a sinusoid half-wave with a duration of $\tau = 1$ ms and an amplitude up to 38 kOe. The large amplitude of the field led to the formation of a flat top of the generated voltage pulse because of saturation of the magnetostriction (Fig. 29a). Due to the wide frequency spectrum of the strain pulse $\lambda(f)$, bending and longitudinal modes of acoustic oscillations were effectively excited in the structure. The field conversion coefficient for the direct-ME effect in the Permendur-PZT structure at resonance frequencies reached a_E≈18 V/(Oe·cm).

The authors of Ref.[115] investigated the direct and converse ME effects upon excitation of a Metglas-PZT planar bilayer with rectangular magnetic and electric field pulses with a duration τ from a few microseconds to tens of milliseconds. Under the action of magnetic field pulses, the composite generated damped voltage oscillations with a frequency equal to the acoustic resonance frequency and an exponentially decreasing DC voltage (Fig. 30a). It was shown that by choosing

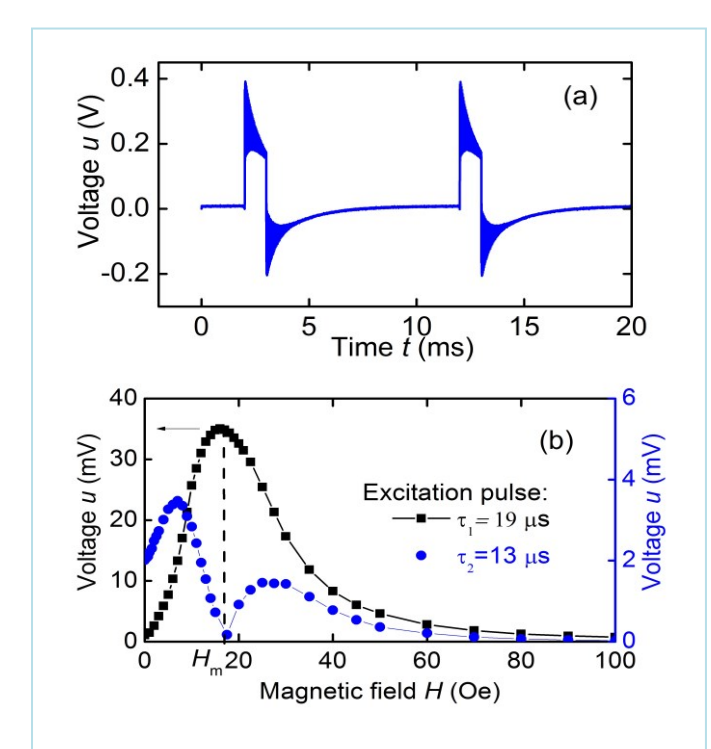


Fig. 30 ME effect in the Metglas-PZT bilayer upon excitation by magnetic field pulses: a) ME response of the structure; b) dependence of the ME pulse amplitude on the field H for the excitation pulses duration of 19 μ m and 13 μ s.

the pulse duration and H, one can selectively excite the linear ME effect or generate the second harmonic of the voltage at the resonance frequency (Fig. 30b). Electric field pulses led to the generation of damped magnetization oscillations at the resonance frequency in a linear or nonlinear regime. The occurrence of nonlinear effects in the regime of pulsed excitation of the structure is due to the nonlinearity of the magnetostriction of the ferromagnetic layer of the structure.

The nonlinear ME effects were studied when a composite of an amorphous ferro-

magnetic film and a piezo-fiber was excited by magnetic field pulses with a duration of $\sim 1-500$ µs and an amplitude up to 50 Oe [116]. Oscillations at the top of generated electric pulse with a period determined by the frequency of longitudinal vibrations of the structure, and the dependence of the pulse amplitude on the bias magnetic bias field H were observed.

To conclude this subsection, we note the work in Ref.[117] where characteristics of the NLME effects in a two-layer structure Metglas-LGT were studied with a change in temperature in the range T=140-350 K. The temperature dependences of the amplitudes of the first three harmonics of ME voltage were measured for H=4 Oe and h=5-15 Oe at 120 Hz. It was shown that the harmonics amplitudes at different h non-monotonically depend on the temperature, which is mainly due to the temperature change in the magnitude of the nonlinear piezomagnetic coefficients $\lambda^{(n)}(T)$ of the Metglas layer.

V DEVICES BASED ON NONLINEAR ME EFFECTS IN COMPOSITES

At present, the most promising application of ME effects in composites is for magnetic field sensors. A variety of sensor designs have been proposed that use linear ME effects [20, 25]. However, in terms of sensitivity and other factors, such sensors cannot yet compete with sensors of other types. This section is devoted to discussion on magnetic field sensors based on NLME effects.

5.1 Sensor of AC magnetic fields based on frequency doubling

In Ref.[118], a sensor for low-frequency magnetic fields was proposed that utilizes the non-resonant ME effect of frequency doubling phenomenon. A composite with a PZT fiber layer sandwiched between two Metglas layers. In the linear mode, when excited by a field h with frequency f, the sensor generated an ME voltage u_1 . In the non-linear mode, the sensor generated a voltage u_2 with a doubled frequency 2f. The amplitude u_2 increased quadratically with h.

Figure 31 shows the dependences $u_1(f)$ for the bias field H=50 Oe and $u_2(f)$ H=0 and h=3 Oe. For comparison, the frequency dependence of the voltage $u_3(f)$ generated in a pickup coil is also shown. The advantage of the ME sensor with frequency doubling is its broadband, high sensitivity

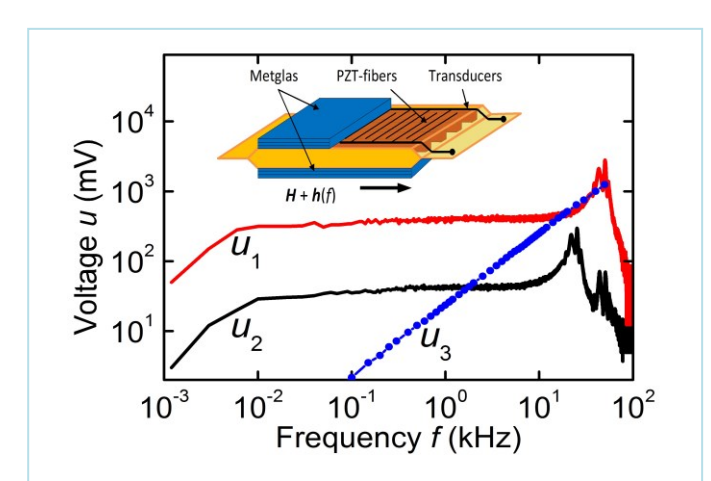


Fig. 31 Dependences of ME voltage on frequency for a magnetic field sensor based on the Metglas-PFC structure: $u_1(f)$ - in linear mode, $u_2(f)$ - in frequency doubling mode, $u_3(f)$ – pickup coil.

in the low-frequency range f < 1 Hz, and operation without a bias field. In the frequency band from ~ 10 Hz to 20 kHz, the sensor sensitivity was ~ 20 mV/Oe, which made it possible to measure fields with amplitudes in the range of 0.1–10 Oe.

5.2 Wideband ME magnetic field sensor

A broadband ME sensor of the heterodyne type was described in Ref.[119], which uses the nonlinear effect of frequency mixing. The sensor is an ME resonator placed in a coil that creates a reference magnetic field h_1 at f_1 . When the measured field h_2 of frequency f_2 acts on the sensor and frequency f_1 is scanned, at the moment when the frequency matching condition $f_2 \pm f_1 = f_0$ is satisfied, the sensor generates a voltage u with a frequency equal to the resonance frequency of the structure f_0 . Based on the known frequency f_1 and the amplitude of the voltage u at resonance, one can determine the amplitude and frequency of the field h_2 .

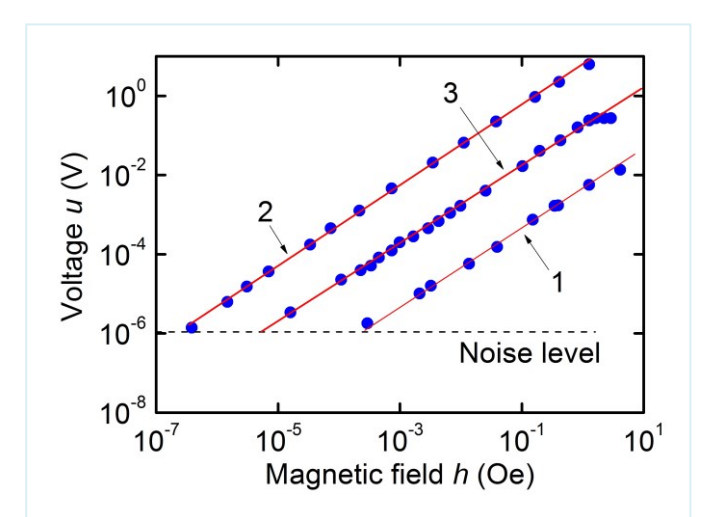


Fig. 32 Dependence of the output voltage u on the measured field h for a field sensor using: 1 - non-resonant linear ME effect, 2 - resonant linear ME effect, 3 - non-linear ME field mixing effect.

The sensor described is based on a Metglas-langatate structure with a resonant frequency $f_0 = 71.15$ kHz and a quality factor $Q\approx1400$ [119]. The sensor operates at $\sim5-80$ kHz and made it possible to register fields with a minimal amplitude $h_1\approx10^{-5}$ Oe. The sensitivity of the sensor was $u/h_1\approx0.2$ V/Oe, which is a factor of 35 higher than the sensitivity of a broadband sensor using a linear non-resonant ME effect, but 40 times smaller than the sensitivity of a narrow-band resonant ME sensor (Fig. 32).

The advantages of the sensor are a wide band of operating frequencies, a linear dependence of the output voltage on the amplitude of the magnetic field, and the absence of a bias field.

5.3 Sensors of low frequency magnetic fields

Many applications require magnetic field sensors operating in the frequency range $f \sim 1\text{-}100$ Hz. However, the sensitivity and dynamic range of linear ME effect sensors in this range are limited by magnetic noise, environmental acoustic noise, and electronic noise, with the noise amplitude increasing as $\sim 1/f$ with decreasing frequency. In 2011–2012, a series of articles appeared

where, in order to reduce the noise limitation, it was proposed to shift the frequency of the measured field upwards, where the noise is much less, and then amplify and demodulate the high-frequency signal [84, 85,120–122].

In Ref. [120], a sensor based on the Metglas-PZT structure with dimensions of 28 mm x 2 mm is described. The sample was placed in a field to be measured with a frequency of 200 Hz and, simultaneously, a modulating field at $f_0 = 10$ –70 kHz and an amplitude h = 1 Oe was applied to it using a coil. The proposed method made it possible to reduce the noise level by a factor of ~70, to ~64.5 nT/ $\sqrt{\text{Hz}}$, and to increase the signal-to-noise ratio by two orders of magnitude, up to 60 dB. This frequency-transfer sensors do not require a magnetizing field, which simplifies their design and allows them to be reduced in size compared to linear ME effect sensors.

A sensor based on a PZT-Metglas composite with a size of 8 cm x 1 cm is described in Ref.[121]. The sample was placed in a measured field with a frequency $f_s = 1$ Hz and a modulating field with a frequency f_m and an amplitude h=0.7 Oe was simultaneously applied. The field frequency f_m was chosen so that the frequency of the side component coincided with the resonance frequency of the structure $f_m \pm f_s = f_0$, where $f_0 = 28.9$ kHz. As a result, compared with a linear

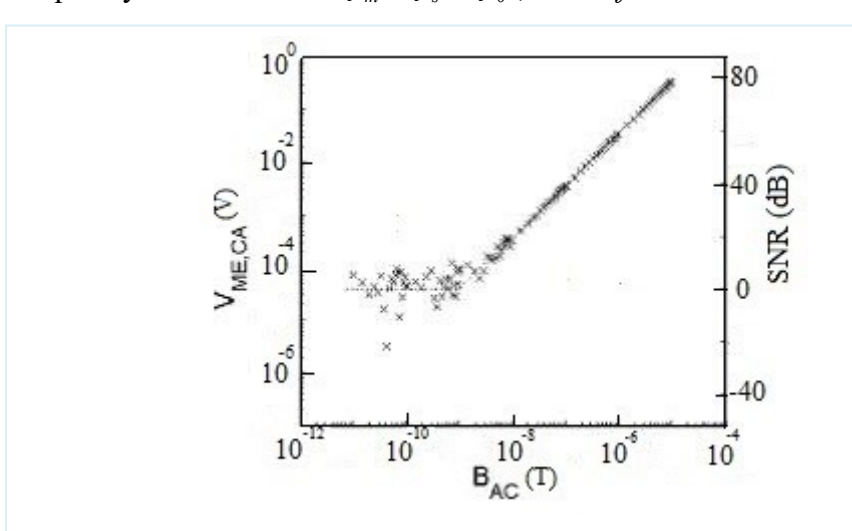


Fig. 33 Sensitivity of the Metglas-AlN modulated sensor at frequency 1 Hz [Reproduced with permission from authors. Ref.122: R. Jahns, H. Greve, E. Woltermann, E. Quandt, R. Knöchel, Sensitivity enhancement of magneto-electric sensors through frequency-conversion. Sens. Actuat. A: Physical **183**, 16–21 (2012).122].

sensor, the minimal detectable field at a frequency of 1 Hz was reduced from 90 pT/\sqrt{Hz} to 7 pT/\sqrt{Hz}, and the signal-tonoise ratio was increased by two

orders of magnitude.

In Ref.[122], a ME sensor based on the Metglas-AlN thin-film structure is described. At a frequency of 1 Hz, the measured field was 1 nT/ $\sqrt{\text{Hz}}$, and the dynamic range reached 80 dB. In sensors based on Metglas-PMN-PT structures, a minimal detectable field was 200 PT at a frequency of 10 mHz and 20 pT at a frequency of 1 Hz [123], minimal spectral noise density was 80 pT/ $\sqrt{\text{Hz}}$ at a frequency of 1 Hz [124] and 100 pT/ $\sqrt{\text{Hz}}$ at a frequency of 0.1 Hz [125].

It was shown [126,127], that field modulation leads to the appearance of additional noise near the resonant frequency, which reduces dynamic range of the sensors, but the noise can be minimized by applying a weak permanent field. It was also shown [128], that the signal-to-noise ratio for frequency-transfer sensors can be significantly increased by optimizing thicknesses of the structure layers.

In Ref. [129] the frequency transfer method was implemented to detect low-frequency magnetic fields using the converse nonlinear ME effect. The authors used a Metglas-AlN thin-film structure and an electric field with a frequency of 515 kHz, equal to the acoustic resonance frequency. As a result of mixing the frequencies of measured magnetic field and the electric field, the spectrum was transferred to the high-frequency region. The value of the registered field was 200 pT/√Hz for a DC field and 70 pT/√Hz for a field with a frequency of 10 Hz. A similar sensor with modulation by an electric field based on the converse ME effect in the Metglas-PMN-PZT structure is described in [130]. The minimum detectable field was ~115 pT at a frequency of 10 Hz and 300 pT at a frequency of 1 Hz. The power consumed by the sensor, 0.56 mW, was significantly smaller than the power ~10−100 mW consumed by other types of sensors.

5.4 Permanent magnetic field sensors

In Ref. [131] a sensor for DC magnetic fields was proposed that uses the nonlinear effect of harmonic generation in an FM-PE structure. The principle of the sensor operation is illustrated in Fig. 34. Under the action of an AC field h and a DC field H(h > H) on the ME structure, it generates

voltage harmonics. The amplitude of the 1st and 3rd harmonics of the voltage increases linearly with increasing H, which is used to measure the DC field. A prototype of the sensor based on the Metglas-PZT-Metglas structure was fabricated. The sensor was excited in a non-resonant mode by h=5 Oe and f=1-10 kHz. The output voltage u_1 was recorded from the piezoelectric layer electrodes at the frequency of the first harmonic. The sensor had a sensitivity of 2.6 V/mT and a range of measured fields from ~ 10 nT to 4 mT. At a high excitation field frequency of f=10 kHz, the sensor made it possible to register not only DC, but also slowly varying fields with frequencies up to ~ 200 Hz.

Similar ME sensor based on the Metglas-langatate-Metglas structure was described in [132]. The sensor was excited harmonically by a field with an amplitude up to h=10 Oe and a frequency of 1.55 kHz. The frequency of the 3rd harmonic of the ME voltage coincided with the frequency of the acoustic bending vibrations of the structure. The voltage generated by the structure was recorded after a narrow-band filter tuned to the resonance frequency. Resonant excitation and the use of the 3rd harmonic made it possible to increase the sensitivity of the sensor and get rid of direct electromagnetic pickup at the excitation frequency. The sensitivity of the sensor to a DC field was 10 V/mT and minimal detectable field was $\sim 1 \text{ nT}$.

The proposed ME magnetometer is a direct ME analogue of flux-gate magnetometers in terms of design and principle of operation. The only difference is that it uses the nonlinearity of magnetostriction $\lambda(H)$ and a piezoelectric layer to record the output signal, while flux-gate magnetometers use the nonlinearity of magnetization M(H) and a coil to record the signal. The advantage of

the ME magnetometer is the ability to increase the sensitivity by 2–3 orders of magnitude by using the resonant excitation mode of the structure, which is not available in flux-gate magnetometers.

Later, a similar DC field sensor based on a Metglas magnetic core of a closed shape and a PMN-

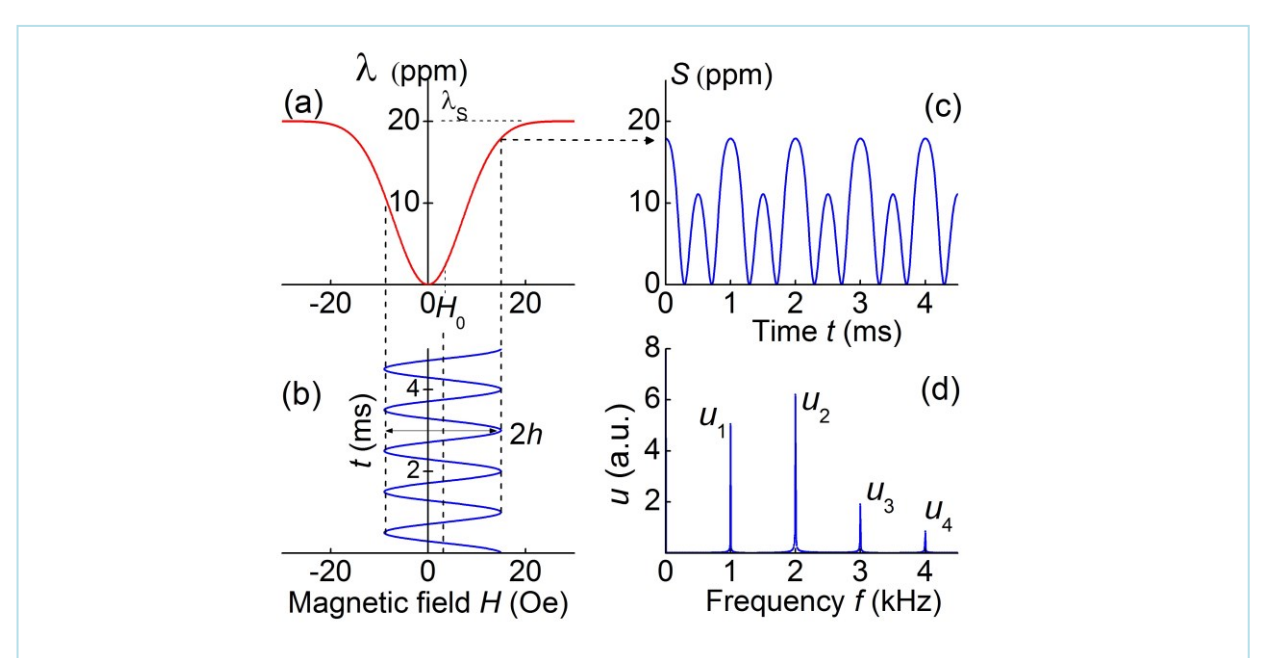


Fig. 34 The figure explains the principle of operation of the DC field ME sensor: (a) dependence of the magnetostriction of the FM layer λ on the magnetic field H; (b) excitation magnetic field; (c) dependence of the deformation of the structure S on time; (d) ME voltage frequency spectrum.

PT piezo-fiber composite was studied in Ref.[133]. The use of a differential scheme for recording the output signal at the first harmonic of the voltage made it possible to obtain a sensitivity of \sim 4.5 V/mT and minimum measured field of \sim 1 nT.

The work reported in Ref.[134] described a similar sensor using the nonlinear ME effect in the Metglas-PZT structure. Upon excitation by a harmonic field at a frequency of 10 kHz and registration of a signal at a frequency of the 3rd harmonic of 30 kHz, which coincides with the frequency of the planar acoustic resonance of the structure, a sensitivity to a DC field of 17.6 V/mT was achieved, and the lowest recorded field was ~2 nT.

In Ref.[135] a DC magnetic field sensor is described that uses a NLME effect and consists of two identical Metglas/Mn-PMN/Metglas structures. Due to the use of the differential scheme for recording the output signal at the frequency of the first harmonic and careful selection of the

structures parameters (which allowed to suppress the second voltage harmonic), when excited by a harmonic field with a frequency of 1 kHz, a sensitivity of 150 V/mT was achieved and the minimum detectable field was 0.8 nT.

5.5 Magnetic field frequency spectrum analyzer

Home appliances and biological organisms generate weak magnetic fields with an amplitude of $10^{-12} - 10^{-4}$ T in the frequency range of $1-10^5$ Hz. The analysis of characteristics of such fields allows obtaining information about the systems in a contactless procedure, as well as conducting medical diagnostics. In Ref.[136], a magnetic field frequency spectrum analyzer is described that uses the NLME effect (Fig.35). The main element of the analyzer is the frequency mixer containing a Metglas-langatate composite. Under the combined action on the structure the analyzed magnetic field $h_1(f)$ and the excitation field $h_2(f_2)$, and the fulfillment of the frequency matching conditions $f_0 = f_1 \pm f_2$, the sensor generates an electric voltage at the acoustic resonance frequency f_0 . Sequential analysis of the spectrum is carried out by tuning the frequency f_2 of the excitation field. An analyzer prototype has been created based on a langatate plate located between two Metglas layers. The prototype operated in the frequency range 0.1-85 kHz, had a frequency resolution of ~40 kHz, a minimum detectable magnetic field of ~50 nT, and a dynamic range of 35 dB.

5.6 Magnetic field sensors with feedback

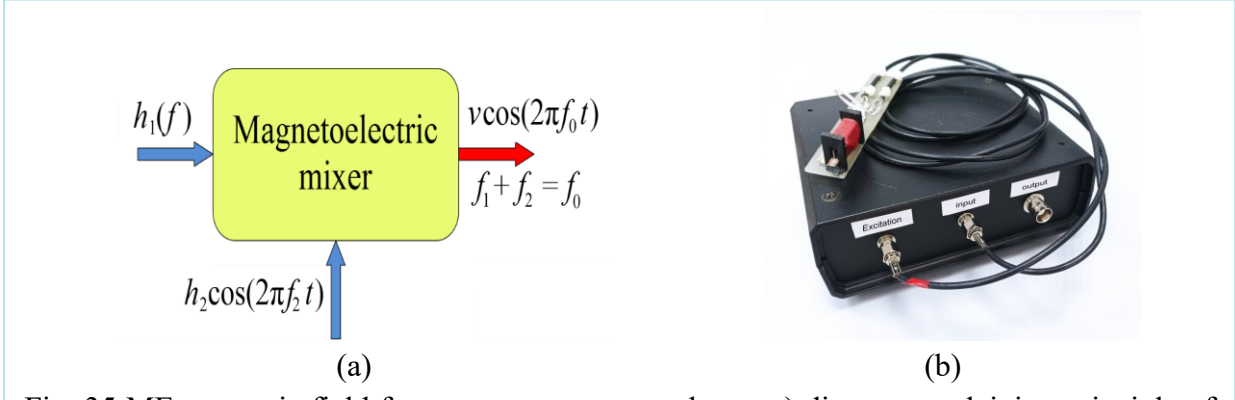


Fig. 35 ME magnetic field frequency spectrum analyzer: a) diagram explaining principle of the device operation, b) picture showing the prototype spectrum analyzer.

To conclude with magnetic field sensors, let us consider a magnetic field sensor containing an amplifier and an ME composite heterostructure in a feedback circuit as in Fig.36, in which the nonlinear characteristics of the ME effect also play an important role. A block-diagram of sensor

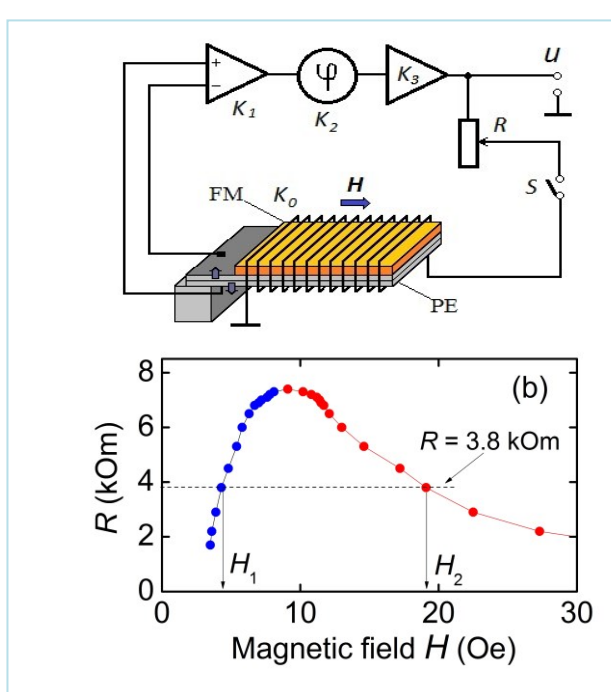


Рис. 36 (a) Block-diagram of the ME generator, (b) dependence of the generation fields region $H_1 < H < H_2$ on the resistance R in the feedback loop.

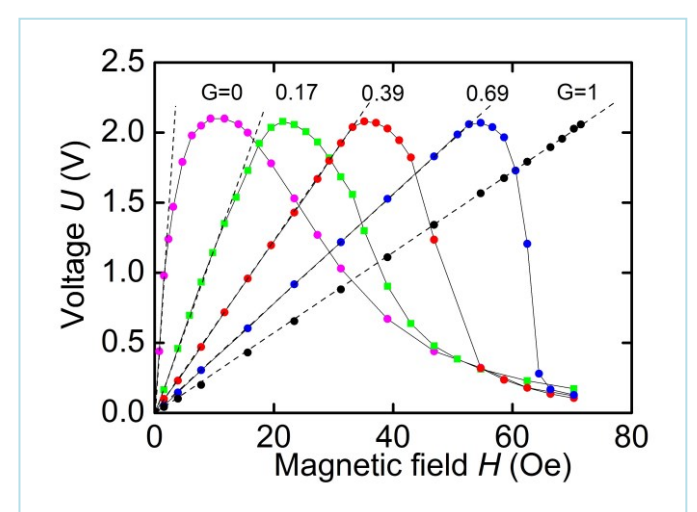


Fig. 37 Dependence of the output voltage U of the ME sensor with negative feedback on the field H for a series of feedback coefficients G.

is shown in Fig. 36a. The sensor contains a broadband amplifier, a phase shifter, a power amplifier, an adjustable voltage divider R, and an ME resonator in the feedback circuit. The ME resonator is magnetized by a DC field H and placed in an electromagnetic coil. When the conditions for the balance of amplitudes and phases are satisfied in a circuit with positive feedback, generation of a voltage occurs at the resonance frequency of the structure f_0 . Amplitude of the generated voltage u depends on the parameters of the amplifier, the voltage division factor and the voltage transfer coefficient of the ME resonator. The resonator transfer coefficient, in turn, depends on the magnetic field *H*. The device generates voltage only in a certain range of magnetic fields $H_1 < H < H_2$, i.e. it can be considered as a threshold magnetic field sensor with an RF output.

The threshold field sensor based on the PZT-Metglas structure was implemented at

a bending vibration frequency of the structure of 2.3 kHz [137]. A similar sensor was implemented using a languate-Metglas composite at the frequency of longitudinal vibrations of the structure at 87.5 kHz [138]. The boundaries of the working fields range of the sensor H_1 and H_2 could be changed from a fraction of Oe to tens of Oe using the voltage divider R.

A device similar to the one in Fig. 36, containing an amplifier, an ME resonator inside the coil and an adjustable voltage divider, with only negative feedback, allows to expand the range of operating fields and linearize the characteristic of the ME field sensor. The scheme was implemented with a Metglas-PZT fiber composite [139]. The field H_c created by the coil in this case is directed towards the measured field H_0 and reduces the magnetic field at the location of the ME resonator $H = H_0 - H_c$. Figure 37 shows the dependences of the output voltage U of the ME sensor on the measured field H as a function of the feedback coefficients of the circuit. It is seen that in this way the linear part of the dependence U(H) was expanded from \sim 1.5 Oe to \sim 72 Oe due to a decrease in the sensitivity of the sensor.

6. CONCLUSION

In conclusion, the review summarizes key efforts on nonlinear ME effects in multiferroic composites that have been studied in detail for the past two decades. Significant progress has been in the understanding of the effects and in both experiments and theory. From the studies discussed in this review, one may draw the following conclusions:

- Nonlinearities of order parameters of the FM and PE materials of multiferroic composites lead to various NLME effects, such as the generation of harmonics, subharmonics, combination frequencies and noise, hysteresis suppression, bistability, parametric amplification, and other effects that manifest at low amplitudes magnetic and electric fields;
- Under the direct ME effect origination from the application of an AC magnetic field, the nonlinearity arises mainly from the dependence of the magnetostriction of the FM layer on the magnetic field $\lambda(H)$;

- Under converse ME effect due to an applied AC electric field, the nonlinearity arises both from the dependence of the PE layer deformation on the electric field $\eta(E)$, and nonlinearity of the magnetostriction of the FM layer;
- The strength of NLME effects increases significantly when the frequencies of the excitation or generated fields coincide with the frequencies of eigen-modes of acoustic oscillations of composite due to the resonant increase in deformations;
- NLME effects were observed in a wide frequency range, from a few Hz to hundreds of kHz in composites with dimensions ranging from hundreds of µm to a few cm;
- The efficiency of NLME assisted field conversion can be controlled by proper choice of applied bias magnetic field *H* and electric field *E*;
- Theories developed so far well describe the main characteristics of NLME effects at relatively small amplitudes of excitation fields. For higher field amplitudes, it is necessary to use numerical calculation methods.
- Various types of highly sensitive sensors of DC and AC magnetic fields have been developed, using the nonlinearity of the direct ME effect in composites.

There are several areas ripe for follow up research. These include:

- Investigation of NLME effects in composites with various connectivity, including core-shell composites [14];
- -Investigation of NLME effects in one and two-dimensional periodic composite structures [140,141];
- Investigation of NLME effects in composites in the absence of external biasing magnetic and electric fields [142];
- Investigation of dynamic characteristics of NLME effects under excitations by short pulses of magnetic or electric fields [115];
- Investigation of NLME effects in composite of new ferroic materials, including electrostrictors, antiferromagnets, and relaxor ferroelectrics [98,143];

- Investigation of NLME effects in micro- and nanocomposites at high frequencies, from several MHz to GHz.
- Development of new ME devices for electronic and microsystem technology and measuring instruments based on NLME effects in composite heterostructures.

ACKNOWLEDGMENT

The work at RTU MIREA was supported by the Russian Ministry of Science and Education within the framework of the State Assignment for Universities No. FSFZ-2023-0005 and the Project No. 075-15-2022-1131. The research at Oakland University was supported by grants from the National Science Foundation (ECCS-1923732, ECCS-EAGER-2236369, DMR-1808892) and the Air Force Office of Scientific Research (AFOSR) Award No. FA9550-20-1-0114.

REFERENCES

- 1. P. Curie, Sur la symetrie dans les phenomenes physiques symetrie d'un champ electrique et d'un champ magnetique. J. Physique 3, 393–415, (1894)
- 2. D.N. Astrov, The magnetoelectric effect in antiferromagnetics, Sov. Phys. JETP **11**, 708–709. (1960).
- 3. G.T. Rado, V.J. Folen, Observation of the magnetically induced magnetoelectric effect and evidence of antiferromagnetic domains. Phys. Rev. Lett. 7, 310–311 (1961).
- 4. Fiebig, M. Revival of the magnetoelectric effect. J. Phys. D Appl. Phys. **38**, R123–R152 (2005).
- 5. J. Scott, Room-temperature multiferroic magnetoelectrics, NPG Asia Materials **5**, e72; (2013). doi:10.1038/am.2013.58.
- 6. H. Schmid, Some symmetry aspects of ferroics and single phase multiferroics, J. Phys. Condens. Matter **20**, 434201 (2008). https://doi.org/10.1088/0953-8984/20/43/43420
- 7. A.P. Pyatakov, A.K. Zvezdin, Magnetoelectric and multiferroic media, Phys.-Usp. 55, 557 (2012). doi 10.3367/UFNe.0182 .201206b.0593
- 8. J. Van Suchtelen, Product properties: A new application of composite materials. Philips Res. Rep. **27**, 28-37 (1972).
- 9. J. van den Boomgaard, A. M. J. G. Van Run, and J. Van Suchtelen, Magnetoelectricity in piezoelectric-magnetostrictive composites, Ferroelectrics **10**, 295 (1976)
- 10. J. Ma, J. Hu, Z. Li, and C.-W. Nan. Recent progress in multiferroic magnetoelectric composites: from bulk to thin films. Advanced materials **23**(9), 1062-1087 (2011). doi.org/10.1002/adma.201003636
- 11. G. Srinivasan, E.T. Rasmussen, J. Gallegos, R. Srinivasan, Y.I. Bokhan, V.M. Laletin, Magnetoelectric bilayer and multilayer structures of magnetostrictive and piezoelectric oxides. Phys. Rev. B **64** (21), 214408 (2001). doi.org/10.1103/PhysRevB.64.214408
- 12. C.-W. Nan, M.I. Bichurin, S. Dong, D. Viehland, G. Srinivasan, Multiferroic magnetoelectric composites: Historical perspective, status, and future directions, J. Appl. Phys. **103**, 031101 (2008). https://doi.org/10.1063/1.2836410

- 13. J.-M. Hu, J. Ma, J. Wang, Z. Li, Y.-H. Lin, C.-W. Nan, Magnetoelectric responces in multiferroic composite thin films, J. Advanced Dielectrics 1, 1-16 (2011) doi: 10.1142/S2010135X11000021
- D. Viehland, J.F. Li, Y. Yang, T. Costanzo, A. Yourdkhani, G. Caruntu, P. Zhou, T. Zhang, T. Li, A. Gupta, M. Popov, G. Srinivasan, Tutorial: Product properties in multiferroic nanocomposites, J. Appl. Phys. 124, 061101 (2018); doi: 10.1063/1.5038726
- M. Bichurin, D. Filippov, V. Petrov, V. Laletsin, N. Paddubnaya, G. Srinivasan, Resonance magnetoelectric effects in layered magneto-strictive-piezoelectric composites, Phys. Rev. B 68, 10-13 (2008). https://doi.org/10.1103/PhysRevB.68.132408
- 16. H. Palneedi, V. Annapureddy, S. Priya, J. Ryu, Status and perspectives of multiferroic magnetoelectric composite materials and applications, Actuators 5, 9 (2016). doi:10.3390/act5010009.
- 17. G. Srinivasan, Layered multiferroic composites, In book: Composite Magnetoelectrics, by G Srinivasan, S Priya, N Sun 2015. doi 10.1016/B978-1-78242-254-9.00003-2
- M.M. Vopson, Fundamentals of multiferroic materials and their possible applications, Critical Review in Solid State and Materials Sciences, 0: 1-28. (2014).
 DOI: 10.1080/10408436.2014.992584
- 19. Y. Wang, J. Li, D. Viehland Magnetoelectrics for magnetic sensor application: status, challenges and perspectives, Mater. Today, **17**, 269 (2014). doi:10.1016/j.mattod.2014.05.004
- 20. M. Bichurin, R. Petrov, O. Sokolov, V. Leontiev, V. Kuts, D. Kiselev, Y. Wang, Magnetoe-lectric magnetic field sensors: A review, Sensors **21**, 6232 (2021). doi.org/10.3390/s21186232
- 21. X. Liang, H. Chen, N.X. Sun, Magnetoelectric materials and devices, APL Mater. **9**, 041114 (2021). doi: 10.1063/5.0044532.
- 22. N. Pereira, A.C. Lima, S. Lanceros-Mendez, P. Martins, Magnetoelectrics: Three centuries of research heading towards the 4.0 industrial revolution. Materials **13**, 4033 (2020). doi:10.3390/ma13184033
- 23. D.R. Patil, A. Kumar, J. Ryu, Recent progress in devices based on magnetoelectric composite thin films, Sensors **21**, 8012 (2021). https://doi.org/10.3390/s21238012
- 24. Q. Mao, J. Wu, Z. Hu, Y. Xu, Y. Du et al, Magnetoelectric devices based on magnetoelectric bulk composites. J. Mater. Chem. C, **9**, 5594 (2021). doi 10.1039/D1TC00419K
- 25. J.-M. Hu, C.-W. Nan, Opportunities and challenges for magnetoelectric devices, APL Mater. 7, 080905 (2019). doi: 10.1063/1.5112089
- 26. Bukharaev A.A., Zvezdin A.K., Pyatakov A.P., Fetisov Y.K., Straintronics: a new trend in micro, nanoelectronics and materials science, Physics Uspekhi **61**(12), 1175 (2018). DOI 10.3367/UFNe.2018.01.038279
- 27. C. M. Leung, J. Li, D. Viehland, X Zhuang, A review on applications of magnetoelectric composites: from heterostructural uncooled magnetic sensors, energy harvesters to highly efficient power converters J. Phys. D: Appl. Phys. **51**, 263002 (2018) doi 10.1088/1361-6463/aac60b
- 28. B.D. Cullity and C.D. Graham, Introduction to magnetic materials, Willey-IEEE Press, 2-d Edition, 2008, 568 p. DOI:10.1002/9780470386323
- 29. Magnetostriction. *Theory and applications of magnetoelesticity*. E. du Tremolet de Lacheisserie, CRC Press; 1st edition (June 9, 1993), 432 p.
- 30. Y.K. Fetisov, D.V. Chashin, N.A Ekonomov, D.V. Burdin, L.Y. Fetisov, Correlation between magnetoelectric and magnetic properties of ferromagnetic-piezoelectric structures, IEEE Trans. Magn. **51**(11), 7120129 (2015). doi:10.1109/INTMAG.2015.7157354
- 31. D.A. Hall, Review of nonlinearity in piezoelectric ceramics, J. Mater. Sci. **36**, 4575-4601 (2001). https://doi.org/10.1023/A:1017959111402

- 32. N.B. Gharb, S. Trolier-McKinstry, D. Damjanovic, Piezoelectric nonlinearity in ferroelectric thin films. J. Appl. Phys. **100**(4), 044107 (2006). doi:10.1063/1.2266235
- 33. M. Bloembergen, *Nonlinear optics*, World Scientific Publishing Company; 4th ed. edition (January 1, 1996), 188 p.
- 34. V. I. Ozhogin, V. L. Preobrazhenskii, Unharmonicity of mixed modes and giant acoustic nonlinearity of antiferromagnets, Sov. Phys. Usp. **31**, 713 (1988). doi: 10.1070/pu1988v031n08abeh004908
- 35. K.E. Kamentsev, Y.K. Fetisov, G. Srinivasan, Low-frequency nonlinear magnetoelectric effects in a ferrite-piezoelectric multilayer, Appl. Phys. Lett. **89**, 142510 (2006). https://doi.org/10.1063/1.2360239
- 36. R.M. Bozorth. Ferromagnetism. D. Van Nostrand, Inc., 1968.
- 37. G. Srinivasan, C.P. De Vreugd, V.M. Laletin, N. Pjddubnaya, M.I. Bichurin, V.M. Petrov, D.A. Filippov, Resonant magnetoelectric coupling in trilayers of ferromagnetic alloy and piezoelectric lead zirconate titanate: The influence of bias magnetic field, Phys. Rev. B **71** 184423 (2005). DOI: 10.1103/PhysRevB.71.184423
- 38. M.H. Seavey, Acoustic resonance in the easy-plane weak ferromagnets α–Fe₂O₃ and FeBO₃, Solid State Commun. **10**, 219-223 (1972). doi.org/10.1016/0038-1098(72)90385-737.
- 39. P. Svec, R. Szewczyk, J. Salach, D. Jackiewicz, P. Svec, A. Bienkowski, J. Hosko. Magnetoelastic properties of selected amorphous systems tailored by thermomagnetic treatment, J. Electr. Engin. **65**(4), 259–261 (2014). doi: 10.2478/jee-2014-0040
- 40. https://metglas.com/magnetic-materials/
- 41. X. Liang, C. Dong, H. Chen, J. Wang, Y. Wei, M. Zaeimbashi, Y. He, A. Matyushov, C.Sun, N. Sun, A review of thin-film magnetoelastic materials for magnetoelectric applications. Sensors **20**(5), 1532 (2020). doi:10.3390/s20051532
- 42. J. Atulasimha, A.B. Flatau, A review of magnetostrictive iron–gallium alloys. Smart Materials and Structures **20**(4), 043001 (2011). doi:10.1088/0964-1726/20/4/043001
- 43. http://tdvib.com/terfenol-d/
- 44. S. R. Murthy and T.S. Rao, Magnetostriction of Ni-Zn and Co-Zn ferrites, **90**, 631-636 (1985) Ed. Görlich, Berlin, Boston: De Gruyter, doi.org/10.1515/9783112494806-025
- 45. L.Y. Fetisov, D.V. Saveliev, M.V. Dzhaparidze, V.I. Musatov, Y.K. Fetisov, Magnetoelectric effect in a flexible structure magnetostriction fiber composite piezopolymer PVDF, Appl. Phys. Lett. **119**, 252904 (2021). doi: 10.1064/5.0076696
- 46. B. Jaffe, W. R. Cook Jr. and H. Jaffe, Piezoelectric Ceramics, Academic Press, New York (1971).
- 47. Y.K. Fetisov, L.Y. Fetisov, G. Srinivasan, Influence of bias electric field on magnetoelectric interactions in ferromagnetic-piezoelectric layered structures, Appl. Phys. Lett. **94**, 132507 (2009). doi 10.1063/1.3114406.
- 48. S. Zhang, F. Li, High performance ferroelectric relaxor-PbTiO3 single crystals: Status and perspective, J. Appl. Phys. **111**, 031301 (2012). doi:10.1063/1.3679521
- 49. https://www.americanpiezo.com/
- 50. P. Martins, S. Lanceros-Méndez. Polymer-Based Magnetoelectric Materials, Advanced functional materials **23**(27), 3371-3385 (2013). doi.org/10.1002/adfm.201202780
- 51. G. Sreenivasulu, L.Y. Fetisov, Y.K. Fetisov, G. Srinivasan. Piezoelectric single crystal langatate and ferromagnetic composites: Studies on low-frequency and resonance magnetoelectric effects. Appl. Phys. Lett. **100**, 0529012012. https://doi.org/10.1063/1.3679661
- 52. G. Sreenivasulu, V.M. Petrov, L.Y. Fetisov, Y.K. Fetisov, G. Srinivasan, Magnetoelectric interactions in layered composites of piezoelectric quartz and magnetostrictive alloys, Phys. Rev. **86**, 214405 (2012), doi: 10.1103/PhysRevB.86.214405.
- 53. P. Hayes, V. Schell, S. Salzer, D. Burdin, E. Yarar, A. Piorra, R. Knöchel, Y.K. Fetisov, and E. Quandt. Electrically modulated magnetoelectric AlN/FeCoSiB film composites for DC magnetic field sensing, J. Phys. D: Appl. Phys. 51, 354002 (2018), doi.org/10.1088/1361-6463/aad456

- 54. E. Yarar, V. Hrkac, C. Zamponi, A. Piorra, L. Kienle, E. Quandt, Low temperature aluminum nitride thin films for sensory applications. AIP Advances, **6**(7), 075115 (2016). doi:10.1063/1.4959895
- 55. https://www.smart-material.com/
- 56. F. Li, L. Jin, Z. Xu, and S. Zhang, Electrostrictive effect in ferroelectrics: An alternative approach to improve piezoelectricity, Appl. Phys. Rev. 1, 011103(2014). doi: 10.1063/1.4861260.
- 57. A.L. Kholkin, E.K. Akdogan, A. Safari, P.-F. Chauvy, N. Setter, Characterization of the effective electrostriction coefficients in ferroelectric thin films. J. Appl. Phys. **89**(12), 8066 (2001). doi:10.1063/1.1371002
- 58. D.A. Burdin, D.V. Chashin, N.A. Ekonomov, L.Y. Fetisov, Y.K. Fetisov, G. Srinivasan G. Sreenivasulu, Nonlinear magnetoelectric effects in planar ferromagnetic-piezoelectric structures, JMMM 358–359, 98-104 (2014). doi.org/10.1016/j.jmmm.2014.01.062
- 59. L.Y. Fetisov, D.A. Burdin, N.A. Ekonomov, D.V. Chashin, J. Zhang, G. Srinivasan, and Fetisov Y. K. Nonlinear magnetoelectric effects at high magnetic field amplitudes in composite multiferroics, J. Phys. D: Appl. Phys. **51**(15), 15400321 (2018). doi 10.1088/1361-6463/aab384
- 60. Y. Wang, Y. Shen, J. Gao, M. Li, J. Li et al. Nonlinear magnetoelectric response of a Metglas/piezofiber laminate to a high-frequency bipolar AC magnetic field action: Appl. Phys. Lett. **102**, 102905 (2013). doi: 10.1063/1.4795307
- 61. Y. Shi, N. Li, Y. Wang, J. Ye, An analytical model for nonlinear magnetoelectric effect in laminated composites. Comp. Struc. **263**, 113652 (2021). doi.org/10.1016/j.compstruct.2021.113652
- 62. S. Timoshenko, *Vibration Problems in Engineering*, D. Van Nostrand Company Inc., Toronto, 1955, p. 310.
- 63. J. A. Osborn, Demagnetizing factors of the general ellipsoid, Phys. Rev. 67, 351–357 (1945).
- 64. D. X. Chen, E. Pardo, A. Sanchez, Demagnetizing factors of rectangular prisms and ellipsoids, IEEE Trans. Magn. **38**, 1742-1752 (2012). doi: 10.1109/TMAG.2002.1017766
- 65. M.I. Bichurin, V.M. Petrov, G. Srinivasan, Theory for low-frequency magnetoelectric coupling in magnetostrictive-piezoelectric bilayers, Phys. Rev. B **68**, 054402 (2003). Doi: 10.1103/PhysRevB.68.054402
- 66. S. Dong, J.-F. Li, and D. Viehland, Longitudinal and transverse magnetoelectric voltage coefficients of magnetostrictive/piezoelectric laminate composite: Theory, IEEE Trans. on UFFC 50(10), 1253-1261 (2003). doi: 10.1109/TUFFC.2003.1244741
- 67. Vopson M.M., Fetisov Y.K., Caruntu G., Srinivasan G. Measurement technique of the magneto-electric coupling in multiferroics. Materials **10**, 963 (2017). doi:10.3390/ma10080963
- 68. K. E. Kamentsev, Y. K. Fetisov, and G. Srinivasan, Ultralow-frequency magnetoelectric effect in a multilayer ferrite–piezoelectric structure, Techn. Phys. **52**(6), 727–733 (2007). doi: 10.1134/S1063784207060084.
- 69. Y. Wang, Y. Shen, J. Gao, M. Li, J. Li, D. Viehland, Nonlinear magnetoelectric response of a Metglas/piezofiber laminate to a high-frequency bipolar AC magnetic field, App. Phys. Lett. **102**, 102905 (2013). https://doi.org/10.1063/1.4795307
- 70. V.M. Laletin, V.M. Petrov, Nonlinear magnetoelectric response of a bulk magnetostrictive—piezoelectric composite, Solid State Commun. **151**, 1806–1809 (2011) doi:10.1016/j.ssc.2011.08.021
- 71 J. Ma, Z. Li, Y. Lin, C.-W. Nan, A novel frequency multiplier based on magnetoelectric laminate, J. Mag. Magn. Mater. **323**, 101-103 (2011). doi:10.1016/j.jmmm.2010.08.039
- 72. J. Gao, Y. Shen, P. Finkel, J. Blottman, J. Li, D. Viehland, Geomagnetic field tuned frequency multiplication in Metglas/Pb(Zr,Ti)O3 heterostructure, Mater. Lett. **88**, 47-50 (2012). doi:10.1016/j.matlet.2012.08.062

- 73. Y. Shen, J. Gao, Y. Wang, P. Finkel, J. Li, D. Viehland, Pezomagnetic strain dependent non-linear magnetoelectric response enhancement by flux concentration effect, Appl. Phys. Lett. **102**, 172904 (2013); doi: 10.1063/1.4803660.
- 74. W. Zhang, G. Yin, J. Cao, J. Bai, F. Wei, Frequency multiplying behavior in a magnetoelectric unimorph. Appl. Phys. Lett. **100**(3), 032903 (2012). Doi: 032903. doi:10.1063/1.3678635.
- 75 L.Y. Fetisov, Y.K. Fetisov, G. Sreenivasulu, G. Srinivasan, Nonlinear resonant magnetoelectric interactions and efficient frequency doubling in a ferromagnetic-ferroelectric layered structure, J. Appl. Phys. **113**, 116101, (2013). doi.org/10.1063/1.4798579
- 76. Y.K. Fetisov, Nonlinear magnetoelectric interactions in composite multiferroic heterostructures, Bull. Rus. Acad. Scien. Phys. **78**(2), 180-182 (2014). DO10.3103/S1062873814020129
- 77. D.A. Filippov, V.M. Laletin, T.O. Firsova, Nonlinear magnetoelectric effect in composite multiferroics. Phys. Solid State **56**(5), 980–984 (2014). doi:10.1134/S1063783414050096
- 78. H. Xu, Y. Pei, D. Fang, P. Wang, Nonlinear harmonic distortion effect in magnetoelectric laminate composites. Appl. Phys. Lett. **105**(1), 012904 (2014). doi:10.1063/1.4887373
- 79. L.Y. Fetisov, L.A. Baraban, Y.K. Fetisov, D.A. Burdin, M.M. Vopson, Nonlinear magnetoe-lectric effect in flexible composite ferromagnetic-piezopolimer structures, JMMM **441**, 628-634 (2017). doi.org/10.1016/j.jmmm.2017.06.013
- 80. Y.K. Fetisov, D.V. Chashin, D.V. Saveliev, M.S. Afanas'ev, I.G. Simonov-Emel'yanov, M.M. Vopson, Y.K. Fetisov, Magnetoelectric direct and converse resonance effects in a flexible ferromagnetic-piezoelectric polymer structure, J. Magn. Mag. Mater. 485, 251–256 (2019) https://doi.org/10.1016/j.jmmm.2019.04.085.
- 81. D.A. Burdin, D.V. Chashin, N.A. Ekonomov, G. Srinivasan, Y.K. Fetisov, Low-frequency resonant magnetoelectric effects in a planar heterostructure of ferromagnetic yttrium iron garnet film and piezoelectric quartz, J. Mag. Magn. Mater. **59**, 170476 (2022). doi.org/10.1016/j.jmmm.2023.170476
- 82. Y.-W. Gao, J.-J. Zhang, Nonlinear magneto-electric response of a giant magnetostrictive/pie-zoelectric composite cylinder. Acta Mech. Sin. **28**(2), 385–392 (2012). doi:10.1007/s10409-012-0002-1
- 83. D.V. Savelev, F.A. Fedulov, V.I. Musatov, D. A. Burdin, E.V. Bolotina, L.Y. Fetisov, Y.K. Fetisov, Nonlinear resonant magnetoelectric effect in a circumferentially magnetized ferromagnetic-piezoelectric ring heterostructure, Appl. Phys. Lett. **122**, 192902 (2023). doi.org/10.1063/5.0146511
- 84. L. Shen, M. Li, J. Gao, Y. Shen, J. F. Li, D. Viehland, X. Zhuang, C. Lam, C. Cordier, S. Saez, C. Dolabdjian, Magnetoelectric nonlinearity in magnetoelectric laminate sensors. J. Appl. Phys. **110**(11), 114510 (2011). doi:10.1063/1.3665130
- 85 X. Zhuang, M.L.C Sing, C. Cordier, S. Saez, C. Dolabdjian, L. Shen, J.F. Li, M. Li, D. Viehland, Evaluation of applied axial field modulation technique on ME sensor input equivalent magnetic noise rejection. IEEE Sens. J. 11(10), 2266–2272 (2011). doi:10.1109/JSEN.2011.2131647
- 86. D.A. Burdin, D.V. Chashin, N.A. Ekonomov, Y.K. Fetisov, L.Y. Fetisov, G. Sreenivasulu, G. Srinivasan, Resonance mixing of ac magnetic fields in a multiferroic composite, J. Appl. Phys. 113, 033902 (2013). doi.org/10.1063/1.4775797
- 87. D.A. Burdin, D.V. Chashin, N.A. Ekonomov, Y.K. Fetisov, Nonlinear magnetoelectric effect in planar ferromagnetic-piezoelectric heterostructure excited by transverse magnetic field, Appl. Phys. Lett. **116**, 072901 (2019). doi.org/10.1063/1.5136088

- 88. S. Tiwari, M. Ho, A. Marotto, R.N. Candler, Frequency doubling in wirelessly actuated multiferroic MEMS cantilevers. In 2018 IEEE International Frequency Control Symposium (IFCS) (pp. 1-3). IEEE. DOI: 10.1109/FCS.2018.8597518
- 89. D.A. Burdin, D.V. Chashin, N.A. Ekonomov, S.N. Gordeev, Y.K. Fetisov. Nonlinear magnetoelectric effect in a ferromagnetic-piezoelectric structure induced by rotating magnetic field. Smart materials and Structures **28**, 107001 (2019). DOI 10.1088/1361-665X/ab34e9
- 90. D.A. Burdin, Y.K. Fetisov, D.V. Chashin, N.A. Ekonomov, Nonlinear transformation of magnetic noise in a magnetoelectric structure, Techn. Phys. Lett. **43**(9), 866–869 (2017). DOI: 10.1134/S1063785017090152
- 91. D.A. Burdin, D.V. Chashin, N.A. Ekonomov, Y.K. Fetisov, A. Stashkevich, Nonlinear magnetoelectric effects in a composite ferromagnetic-piezoelectric structure under harmonic and noise magnetic pumping, J. Mag. Magn. Mater. **449**, 505-509 (2018). doi.org/10.1016/j.jmmm.2017.10.096
- 92. D.A. Burdin, N.A. Ekonomov, M.M. Vopson, Y.K. Fetisov, Enhancement of the nonlinear magnetoelectric effect in a ferromagnet-piezoelectric heterostructure due to nonlinearity of magnetization, Appl. Phys. Lett. **118**, 132901 (2021). doi.org/10.1063/5.0045300
- 93. D.A. Burdin, D.V. Chashin, N.A. Ekonomov, Y.K. Fetisov, Static deformation of a ferromagnet in an alternating magnetic field, J. Magn. Mag. Mater. **406**, 216 (2016). doi.org/10.1016/j.jmmm.2015.12.078
- 94. J.L. Prieto, C. Aroca, E. Lopez, M.C. Sanchez, P. Sanchez, Reducing hysteresis in magnetostrictive-piezoelectric magnetic sensors. IEEE Trans. Magn. **34**(6), 3913–3915 (1998). doi:10.1109/20.728303
- 95. Burdin D.A., Chashin D.V., Ekonomov N.A., Fetisov L.Y., Fetisov Y.K., Suppression of non-linear magnetoelectric effect hysteresis in a layered ferromagnetic-piezoelectric structure, J. Mag. Magn. Mater. **449**, 152-156 (2018). doi.org/10.1016/j.jmmm.2017.09.067
- 96. D.A. Burdin, D.V. Saveliev, Y.K. Fetisov, N.A. Ekonomov, D.V. Chashin, Magnetoelectric structure with integrated current carrying electrodes, J. Phys.: Conf. Ser. **1389** 012049 (2019). doi:10.1088/1742-6596/1389/1/012049
- 97. D.A. Burdin, D.V. Savelev, N.A. Ekonomov, D.V. Chashin, Y.K. Fetisov, Effective excitation of magnetoelectric voltage harmonics in a ferromagnet-piezoelectric structure by current passing through the magnetic layer, Techn. Phys. Lett., **46**(5), 487–490 (2020). doi:10.1134/S1063785020050211
- 98. L.Y. Fetisov, D.V. Chashin, D.A. Burdin, G. Srinivasan, Y.K. Fetisov, Nonlinear converse magnetoelectric effects in a ferromagnetic-piezoelectric bilayer. Appl. Phys. Lett. **113**, 212903 (2018). https://doi.org/10.1063/1.5054584
- 99. D.V. Saveliev, Y.K. Fetisov, D.V. Chashin, L.Y. Fetisov, D.A. Burdin, N.A. Ekonomov, Magnetoelectric effects in a layered ferromagnet-electrostrictor heterostructure. J. Mag. Magn. Mater. 466, 219-224 (2018). https://doi.org/10.1016/j.jmmm.2018.07.034
- 100. J. Yu, P.E. Janolin, Defining "giant" electrostriction. J. Appl. Phys. **131**, 170701 (2022). https://doi.org/10.1063/5.0079510
- 101. S.A. Gridnev, M.V. Khakhlenkov, L.Y. Fetisov, The influence of the electric field on the magnetoelectric response of a layered ferromagnet electrostrictor heterostructure, Ferroelectrics **561**, 90-99 (2020). doi.org/10.1080/00150193.2020.1736920
- 102. D.A. Burdin, N.A. Ekonomov, D.V. Chashin, Y.K. Fetisov. S.N. Gordeev, Magnetoelectric doubling and mixing of electric and magnetic field frequencies in a layered multiferroic heterostructure. J. Magn. Mag. Mater. 485, 36-42 (2019). DOI: 10.1016/j.jmmm.2019.04.037

- 103. L.Y. Fetisov, D.V. Chashin, Resonance magnetoelectric effects in a layered composite under magnetic and electrical excitation, J Appl. Phys. **112**, 014103. (2012). doi.org/10.1063/1.4733466.
- 104. D.A. Burdin, D.V. Chashin, N.A. Ekonomov, V. L. Preobrazhenskii, S.N. Gordeev, and Y.K. Fetisov Parametric generation of subharmonics in a composite multiferroic resonator, Phys. Rev. Appl. 13, 054070 (2020). doi.org/10.1103/PhysRevApplied.13.054070
- 105. D.A Burdin, N. A Ekonomov, V. L Preobrazhenskii, Y.K Fetisov, Noise generation in a bilayer ferromagnet-piezoelectric heterostructure at the converse magnetoelectric effect. J. Phys. D: Appl. Phys. 55, 015001 (2022). DOI 10.1088/1361-6463/ac28be
- 106. T.-D. Onuta, Y. Wang, C.J. Long, S.E. Lofland, I. Takeuchi, Dynamic state switching in nonlinear multiferroic cantilevers, Appl. Phys. Lett. **102**, 043506 (2012). doi.org/10.1063/1.4738991
- 107. Y.K. Fetisov, D.A. Burdin, N.A. Ekonomov, L.Y. Fetisov, A.A. Berzin, P. Hyes, E. Quandt, Bistability in a multiferroic composite resonator, Appl. Phys. Lett. **113**, 022903 (2018). https://doi.org/10.1063/1.5032182
- 108. Z. Chu, C. Dong, C. Tu et al. Voltage-driven nonlinearity in magnetoelectric heterostructures. Phys. Rev. Appl. 12(4), 044001 (2019). doi:10.1103/PhysRevApplied.12.044001
- 109. Z. Chu, J. Gao, Z. Sun, Z. Mao, S. Zhang, Y. Shen, S. Dong. Jumping and hysteresis effect in 1–1-typed magnetoelectric resonators, Appl. Phys. Lett. **119**, 182901 (2021). doi: 10.1063/5.0066173
- 110. Y. Wang, T. Onuta, C. Long, Y. Geng, I. Takeuchi, Colossal magnetoelectric effect induced by parametric amplification. Appl. Phys. Lett. **107**(19), 192902 (2015). doi:10.1063/1.4935332 royalsocietypublishing.org/journal/rspa
- 111. D.A. Burdin, D.V. Chashin, N.A. Ekonomov, Y.K. Fetisov, Parametric amplification of magnetoacoustic oscillations in a ferromagnet-piezoelectric structure, Techn. Phys. Lett. 46, 200-2002 (2020). Doi: 10.1134/S1063785020020169
- 112. A.Y. Ostashchenko, K.E. Kamentsev, Y.K. Fetisov, G. Srinivasan, Magnetoelectric response of a multilayer ferrite-piezoelectric structure to magnetic field pulses, Techn. Phys. Lett. **30**(9), 769–771 (2004). doi:10.1134/1.1804591
- 113. Y.K. Fetisov, K.E. Kamentsev, A.Y. Ostashchenko, G. Srinivasan, Wide-band magnetoelectric characterization of a ferrite-piezoelectric multilayer using a pulsed magnetic field. Sol. St. Comm. **132**(1), 13–17 (2004). doi:10.1016/j.ssc.2004.07.019
- 114. F. Kreitmeier, D.V. Chashin, L.Y. Fetisov, Y.K. Fetisov, I. Schulz, G.J. Monkman, M. Shamonin, Nonlinear magnetoelectric response of planar ferromagnetic-piezoelectric structures to sub-millisecond magnetic pulses, Sensors **12**(11) 14821-14837 (2012). doi.org/10.3390/s121114821
- 115. D.V. Saveliev, L.Y. Fetisov, D.V. Chashin, V.O. Belan, Y.K. Fetisov. Magnetoelectric effects in a composite ferromagnet-piezoelectric heterostructure under pulsed excitation. J. Phys. D: Appl. Phys. **55**, 485002 (2022). DOI 10.1088/1361-6463/ac962d
- 116. C. Lu, H. Zhou, A. Yang, Z. Ou, F. Yu, H. Gao. Nonlinear magnetoelectric response of Fe73.5Cu1Nb3Si13.5B9/piezofiber composite for a pulsed magnetic field sensor, Materials, 12, 2866 (2019). doi:10.3390/ma12182866
- 117. D. Burdin, N. Ekonomov, D. Chashin, Y. Fetisov, Temperature characteristics of the nonlinear magnetoelectric effect, EPJ Web of Conf. **185**, 07004 (2018). doi.org/10.1051/epjconf/201818507004
- 118. F.A. Fedulov, L.Y. Fetisov, Y.K. Fetisov, A.V. Makovkin, Magnetic field sensor based on magnetoelectric effect of frequency doubling in a ferromagnetic—piezoelectric structure, Nano- and microsystem engineering 6, 59-62 (2015).

- 119. Y.K. Fetisov, D.A. Burdin, D.V. Chashin, N.A. Ekonomov, High-sensitivity wideband magnetic field sensor using nonlinear resonance magnetoelectric effect. IEEE Sens. J. 14, 2252-2256 (2014).
- 120. S. M. Gillette, A. L. Geiler, D. Gray, D. Viehland, C. Vittoria, V. G. Harris, Improved sensitivity and noise in magneto-electric magnetic field sensors by use of modulated ac magneto-striction. IEEE Magn. Lett. **2**, 2500104–2500104 (2011). 10.1109/lmag.2011.2151178
- 121 . J. Petrie, D. Viehland, D. Gray, S. Mandal, G. Sreenivasulu, G. Srinivasan, A.S. Edelstein, Enhancing the sensitivity of magnetoelectric sensors by increasing the operating frequency. J. Appl. Phys. **110**(12), 124506 (2011). doi:10.1063/1.3668752.
- 122. R. Jahns, H. Greve, E. Woltermann, E. Quandt, R. Knöchel, Sensitivity enhancement of magnetoelectric sensors through frequency-conversion. Sens. Actuat. A: Physical **183**, 16–21 (2012). doi:10.1016/j.sna.2012.05.049
- 123. Y. Liu, J. Jiao, J. Ma, B. Ren, L. Li, X. Zhao, H. Luo, L. Shi, Frequency conversion in magnetoelectric composites for quasi-static magnetic field detection. Appl. Phys. Lett. **103**(21), 212902 (2013). doi:10.1063/1.4832861
- 124. J. Ma, C. Jiao, C. Fang, H. Zhao, H. Luo, High sensitive nonlinear modulation magnetoelectric magnetic sensors with a magnetostrictive metglas structure based on bell-shaped geometry. J. Magn. Mag. Mater. **405**, 225-230 (2016). doi:10.1016/j.jmmm.2015.12.073
- 125. Z. Chu, Z. Yu, M. PourhosseiniAsl, C. Tu, S. Dong, Enhanced low-frequency magnetic field sensitivity in magnetoelectric composite with amplitude modulation method. Appl. Phys. Lett. **114**(13), 132901 (2016). doi:10.1063/1.5087954
- 126. P. Durdaut, S. Salzer, J. Reermann, V. Robisch, J. McCord, D. Meyners, E. Quandt, G. Schmidt, R. Knochel, M. Hoft, Improved magnetic frequency conversion approach for magnetoelectric sensors. IEEE Sens. Lett. 1, 2500104 (2017). doi:10.1109/LSENS.2017.2699559
- 127. S. Salzer, P. Durdaut, V. Röbisch, D. Meyners, E. Quandt, M. Höft, R. Knöchel, Generalized magnetic frequency conversion for thin-film laminate magnetoelectric sensors, IEEE Sensor J. 17(5), 1373-1383 (2017). 10.1109/JSEN.2016.2645707
- 128.Y. Shen, J. Gao, Y. Wang, Y. Li, D. Viehland, High non-linear magnetoelectric coefficient in Metglas/PMN-PT laminate composites under zero direct current magnetic bias. J. Appl. Phys. 115(9), 094102 (2014). doi:10.1063/1.4867516
- 129. Hayes, M.J. Klug, S. Toxvaerd, et al. Converse magnetcoelectric composite resonator for sensing small magnetic field, Sci. Reports 9, 16355 (2019). DOI: 10.1038/s41598-019-52657-
- 130. Z. Chu, C. Dong, C. Tu, X. Liang, H. Chen, C. Sun, Z. Yu, S. Dong, N.X. Sun. A low-power and high-sensitivity magnetic field sensor based on converse magnetoelectric effect. Appl. Phys. Lett. **115**(16), 162901 (2019). doi:10.1063/1.5122774
- 131. D. Burdin, D. Chashin, N. Ekonomov, L. Fetisov, Y. Fetisov, M. Shamonin, D.C. magnetic field sensing based on the nonlinear magnetoelectric effect in magnetic heterostructures, J. Phys. D. Appl. Phys. **49**, 375002 (2016). DOI 10.1088/0022-3727/49/37/375002
- 132. D.A. Burdin, D.V. Chashin, N.A. Ekonomov, Y.K. Fetisov, A.A. Stashkevich High-sensitivity dc field magnetometer using nonlinear resonance magnetoelectric effect, J. Magn. Mag. Mater. 405, 244-248 (2016). https://doi.org/10.1016/j.jmmm.2015.12.079
- 133. Z. Chu, H. Shi, M.J. PourhosseiniAsl, J. Wu, W. Shi, X. Gao, X. Yuan, S. Dong, A magnetoelectric fux gate: new approach for weak DC magnetic feld detection, Scien. Rep. 7, 8592 (2017). DOI:10.1038/s41598-017-09420-w
- 134. M. Li, C. Dong, H. Zhou, Z. Wang, X. Wang, X. Liang, Y. Lin, N.X. Sun, Highly sensitive DC magnetic field sensor based on nonlinear ME effect. IEEE Sensors Letters 1(6), 1–4 (2017). doi:10.1109/LSENS.2017.2752216
- 135. R. Chen, T. Deng, Z. Chen, Y. Wang, W. Di, L. Lu, J. Jiao, H. Luo, Differential configuration for highly sensitive DC magnetic field sensing based on nonlinear magnetoelectric effect, IEEE Sensors J. **22**(18), 17754 (2022). doi: 10.1109/JSEN.2022.3194142

- 136. F.A. Fedulov, L.Y. Fetisov, D.V. Chashin, D.V. Saveliev, D.A. Burdin, Y.K. Fetisov. Magnetic field spectrum analyzer using nonlinear magnetoelectric effect in composite ferromagnet piezoelectric heterostructure. J. Magn. Mag. Mater. 346, 113844 (2022). doi.org/10.1016/j.sna.2022.113844
- 137. Y. K. Fetisov, V.N. Serov, L.Y. Fetisov, S.A. Makovkin, D. Viehland, G. Srinivasan, A magnetoelectric composite based signal generator. Appl. Phys. Lett., 108(21), 213502 (2016). doi:10.1063/1.4952768
- 138. L.Y. Fetisov, V.N. Serov, D.V. Chashin, S.A. Makovkin, G. Srinivasan, D. Viehland, Y.K. Fetisov, A magnetoelectric sensor of threshold DC magnetic fields. J. Appl. Phys. **121**(15), 154503 (2017). doi:10.1063/1.4981533
- 139. N. Serov, D.V. Chashin, L.Y. Fetisov, Y.K. Fetisov, A.A. Berzin, Widening and linearization of dc magnetic field magnetoelectric sensor characteristic using compensation scheme, IEEE Sensors J. **18**(20) 8256-8260 (2018). 10.1109/JSEN.2018.2856300
- 140. F.A. Fedulov, D.A. Saveliev, D.V. Chashin, S.B. Odinokov, A.S. Kuznetsov, Y.K. Fetisov, Anisotropy of magnetoelectric effects in a planar heterostructure comprising piezoelectric substrate and ferromagnetic grating, JMMM 547, 168943 (2022). org/10.1016/j.jmmm.2021.168943
- 141. F.A. Fedulov, D.V. Saveliev, D.V. Chashin, V.I. Shishkin, Y.K. Fetisov Magnetoelectric effects in stripe- and periodic heterostructures based on nickel–lead zirconate titanate bilayers. Rus. Techn. J. **10**(3), 64-73 (2022) doi.org/10.32362/2500-316X-2022-10-3-64-73
- 142. Y. Zhou, D. Maurya, Y. Yan, G. Srinivasan, E. Quandt, S. Priya, Self-biased magnetoelectric composites: An overview and future perspectives. Energy Harvesting and Systems **3**(1), 1-42. (2016). https://doi.org/10.1515/ehs-2015-0003
- 143 .D.A. Burdin, D.V. Chashin, N.A. Ekonomov, L.Y. Fetisov, V.L. Preobrazhensky, Y.K. Fetisov, Low-frequency resonance magnetoelectric effects in layered heterostructures antiferromagnet-piezoelectric, Sensors 23(13), 5901 (2023). doi.org/10.3390/s23135901